CANCER

Matrix-binding checkpoint immunotherapies enhance antitumor efficacy and reduce adverse events

Jun Ishihara,[1,2] Kazuto Fukunaga,[1,2,3]* Ako Ishihara,[1]* Hans M. Larsson,[2] Lambert Potin,[1,2] Peyman Hosseinchi,[1] Gabriele Galliverti,[2] Melody A. Swartz,[1,2,4,5] Jeffrey A. Hubbell[1,2,5]†

Immune checkpoint blockade exhibits considerable antitumor activity, but previous studies have reported instances of severe treatment-related adverse events. We sought to explore local immune checkpoint blockade, with an antibody (Ab) form that would be retained intra- or peritumorally, limiting systemic exposure. To accomplish this, we conjugated the checkpoint blockade Abs to an extracellular matrix (ECM)–super-affinity peptide derived from placenta growth factor–2 (PlGF-$2_{123–144}$). We show enhanced tissue retention and lower Ab concentrations in blood plasma after PlGF-$2_{123–144}$ conjugation, reducing systemic side effects such as the risk of autoimmune diabetes. Peritumoral injections of PlGF-$2_{123–144}$–anti-CTLA4 (cytotoxic T lymphocyte antigen 4) and PlGF-$2_{123–144}$–anti–PD-L1 (programmed death ligand 1) Abs delayed tumor growth and prolonged survival compared to the unmodified Abs in genetically engineered murine tumor models of melanoma and breast cancer. The PlGF-$2_{123–144}$–Abs increased tumor-infiltrating activated $CD8^+$ and $CD4^+$ T cells, resulting in a delay of distant tumor growth as well. This simple and translatable approach of engineered ECM-binding Abs may present a viable and safer approach in checkpoint blockade.

INTRODUCTION

Immune checkpoints are inhibitory pathways used by the immune system to protect host tissues from damage, particularly when the immune system is activated. Recently, these mechanisms have been found to be functionally relevant in cancers for evasion of immune-mediated rejection (*1*, *2*). On the basis of this, immune checkpoint blockade has been demonstrated to be a promising approach for cancer therapy.

Cytotoxic T lymphocyte antigen 4 (CTLA4; CD152) is a transmembrane protein expressed on regulatory T cells (T_{regs}) and activated $CD4^+$ and $CD8^+$ T cells (*3*). It functions as an inducer of immunosuppressive signals by binding to CD80 or CD86 on antigen-presenting cells. Thus, CTLA4 blocking antibodies (Abs) (αCTLA4) can potentiate the activation of effector T cells. In addition, anti-mouse CTLA4 Ab clone 9H10, but not UC-4F10-11 (4F10), depletes T_{regs} through Ab-dependent cell-mediated cytotoxicity, further enhancing its antitumor effects (*4*, *5*). In the clinic, αCTLA4 (ipilimumab) treatment resulted in improved survival of melanoma patients (*6*).

Some tumor cells express programmed death ligand 1 (PD-L1) (CD274 and B7-H1), a key molecule in the pathway to evade immune response via binding to programmed cell death-1 (PD-1) on activated T cells (*7*–*9*). The PD-L1/PD-1 interaction results in decreased cytokine production, inhibition of proliferation, and apoptosis of T cells. Both anti–PD-1 (αPD-1; pidilizumab, pembrolizumab, and nivolumab) and anti–PD-L1 (αPD-L1; atezolizumab and avelumab) blocking Abs have inhibited tumor growth in mouse models and in the clinic (*10*–*12*).

Because the CTLA4 and PD-1/PD-L1 inhibitory pathways are nonredundant, the combination of αPD-L1 and αCTLA4 can have synergistic antitumor effects (*13*). Clinical trials using both nivolumab and ipilimumab showed a prolongation of survival, and these drugs have been approved for melanoma treatment by the U.S. Food and Drug Administration. However, 68.7% of patients showed grade 3 or 4 side effects. In particular, 36.4% of these patients could not continue with the therapy due to treatment-related adverse events (*14*).

Heparin-binding domains (HBDs) in several GFs bind to the HBDs derived from a variety of extracellular matrix (ECM) proteins (*15*–*19*). By screening the binding of GFs to a variety of ECM proteins, we have discovered that the HBD of placenta growth factor–2 (PlGF-$2_{123–144}$) has an exceptionally high affinity for multiple ECM proteins (*20*). We have shown that fusion of the PlGF-$2_{123–144}$ domain to GFs enhanced their tissue retention and therapeutic efficacy in mouse models of skin and bone regeneration (*20*). Here, we engineered immune checkpoint blockade Abs conjugated with PlGF-$2_{123–144}$ peptide for cancer immunotherapy. We hypothesized that the enhanced retention of checkpoint blockade Abs in tissue surrounding the tumor would improve their antitumor efficacy by enhancing T cell activation and decrease the side effects of therapy by lowering systemic exposure after local administration.

RESULTS

PlGF-$2_{123–144}$ peptide–conjugated Abs bind to ECM proteins and their targets

We first examined the capacity of PlGF-$2_{123–144}$–conjugated Abs to bind ECM proteins in vitro. After mixing immunoglobulin G (IgG) Abs with sulfosuccinimidyl-4-(*N*-maleimidomethyl) cyclohexane-1-carboxylate (sulfo-SMCC), the PlGF-$2_{123–144}$ peptide was cross-linked covalently to the Ab (Fig. 1A). SDS–polyacrylamide gel electrophoresis (PAGE) revealed that molecular weights of both light and heavy chains of IgG were increased (Fig. 1B). An average of 6.3 and 6 PlGF-$2_{123–144}$ peptides were bound to monoclonal αCTLA4 (4F10) and monoclonal αPD-L1, respectively, as calculated by matrix-assisted laser desorption/ionization–time-of-flight (MALDI-TOF) mass spectrometry (MS; fig. S1). PlGF-$2_{123–144}$ conjugation did not yield high–molecular

[1]Institute for Molecular Engineering, University of Chicago, Chicago, IL 60637, USA. [2]Institute of Bioengineering, Ecole Polytechnique Fédérale de Lausanne, CH-1015 Lausanne, Switzerland. [3]Department of Bioengineering, Tokyo Institute of Technology, 226-8501 Yokohama, Kanagawa, Japan. [4]Swiss Institute for Experimental Cancer Research, School of Life Sciences, Ecole Polytechnique Fédérale de Lausanne, CH-1015 Lausanne, Switzerland. [5]Institute of Chemical Sciences and Engineering, School of Basic Sciences, Ecole Polytechnique Fédérale de Lausanne, CH-1015 Lausanne, Switzerland.
*These authors contributed equally to this work.
†Corresponding author. Email: jhubbell@uchicago.edu

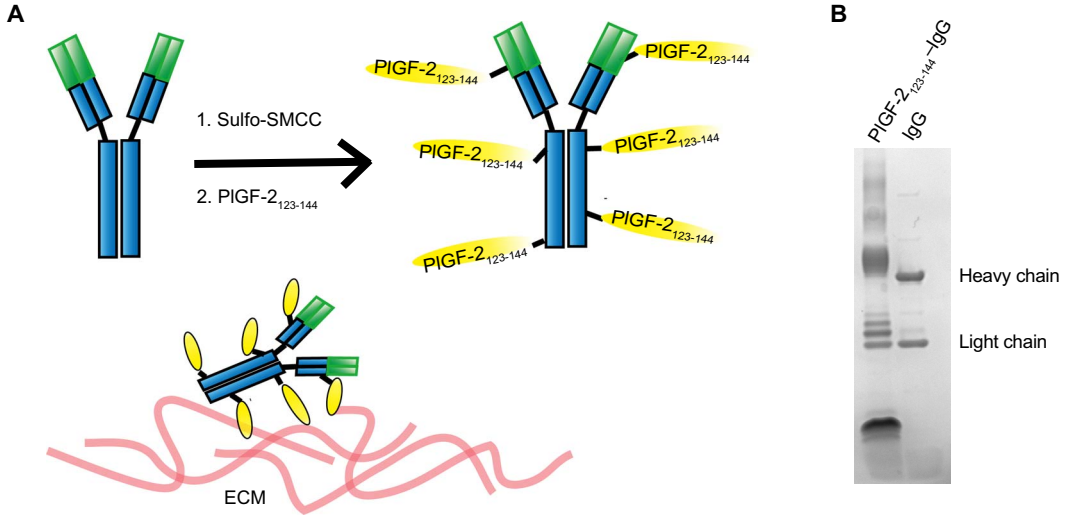

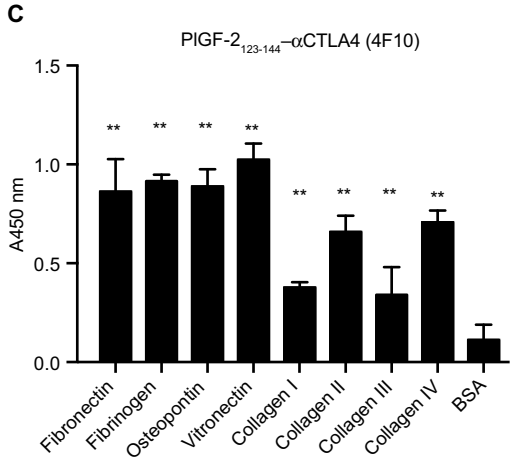

E

K_d (nM)	Fibronectin	Collagen I	rmCTLA4
PlGF-$2_{123-144}$–4F10	4.7	26.7	1.6×10^{-1}
4F10	N.D.	N.D.	1.0×10^{-1}

K_d (nM)	Fibronectin	Collagen I	rmCTLA4
PlGF-$2_{123-144}$–9H10	8.7×10^{-1}	1.3	5.7
9H10	N.D.	N.D.	15

K_d (nM)	Fibronectin	Collagen I	rmPD-L1
PlGF-$2_{123-144}$–αPD-L1	3.7	5.1	1.7×10^{-1}
αPD-L1	N.D.	N.D.	9.5×10^{-2}

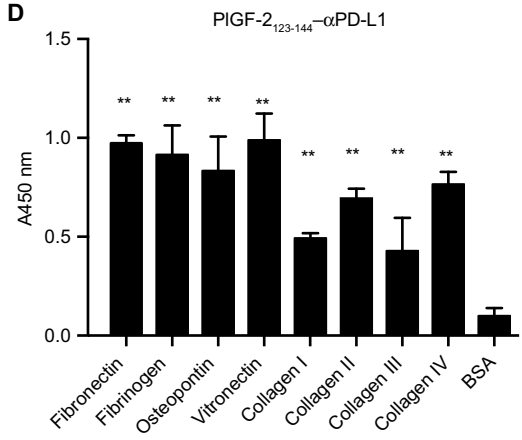

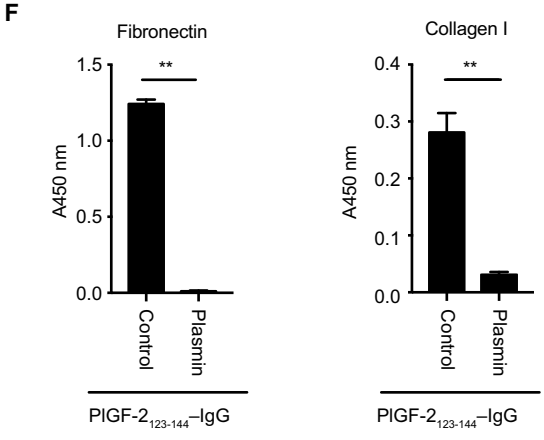

Fig. 1. PlGF-$2_{123-144}$ peptide–conjugated IgG (PlGF-$2_{123-144}$–IgG) binds to ECM proteins with high affinity and is released by plasmin. (**A**) Schematic of conjugation of the PlGF-$2_{123-144}$ peptide to IgG Ab, resulting in binding to ECM proteins. (**B**) PlGF-$2_{123-144}$–rat IgG2a and unmodified rat IgG2a were analyzed by SDS-PAGE under reducing conditions with Coomassie blue staining. (**C**) PlGF-$2_{123-144}$–αCTLA4 (clone UC10-4F10-11: 4F10) and (**D**) PlGF-$2_{123-144}$–αPD-L1 binding to ECM proteins, measured by enzyme-linked immunosorbent assay (ELISA). $A_{450\ nm}$ represents absorbance at 450 nm. Bovine serum albumin (BSA) served as a negative control ($n = 5$, mean ± SD). (**E**) Affinities (K_d values are shown) of PlGF-$2_{123-144}$–αCTLA4 and unmodified αCTLA4 (two clones: 4F10 and 9H10) and αPD-L1 against fibronectin, collagen type I, recombinant mouse CTLA4 (rmCTLA4), and/or rmPD-L1 were measured by ELISA. N.D., not determined because of low signal. Graphs of concentrations versus signal are shown in figs. S4 and S5. (**F**) PlGF-$2_{123-144}$–rat IgG2a lost fibronectin and collagen I binding capacity after plasmin (0.1 U/ml) cleavage, measured by ELISA ($n = 4$, mean ± SD; two experimental repeats). Statistical analyses were done using analysis of variance (ANOVA) with Tukey's test, and a two-tailed Student's t test was used in (F). $^{**}P < 0.01$.

weight aggregates in the final product (fig. S2). Both PlGF-$2_{123–144}$–αCTLA4 and PlGF-$2_{123–144}$–αPD-L1 bound to eight different ECM proteins: fibronectin, fibrinogen, vitronectin, osteopontin, and type I, II, III, and IV collagens. In comparison, neither unmodified αCTLA4 nor unmodified αPD-L1 bound to the tested ECM proteins (Fig. 1, C and D, and fig. S3). Strong binding affinities [nanomolar range dissociation constant (K_d) values] of PlGF-$2_{123–144}$–αCTLA4 (9H10 and 4F10) and PlGF-$2_{123–144}$–αPD-L1 for fibronectin and collagen type I, main components of skin ECM, were observed (Fig. 1E and fig. S4). PlGF-$2_{123–144}$–αCTLA4 and PlGF-$2_{123–144}$–αPD-L1 also recognized their target antigens with similar K_d values to the unmodified Abs (Fig. 1E and fig. S5). Together, these data showed that PlGF-$2_{123–144}$–Abs bind ECM proteins without impairment of their antigen recognition capacities.

PlGF-$2_{123–144}$–Abs lose affinity for ECM proteins by competition with heparin or by plasmin cleavage

We next examined the release of PlGF-$2_{123–144}$–Abs from ECM proteins. Addition of excess heparin reduced PlGF-$2_{123–144}$–IgG binding to fibronectin in a dose-dependent manner, consistent with our previous observations (fig. S6) (*20*). Addition of plasmin deprived PlGF-$2_{123–144}$–IgG of its ECM binding activity, accompanied by mobility shifts in SDS-PAGE (Fig. 1F and fig. S7) (*20*). These data suggest that PlGF-$2_{123–144}$–Abs can be released from ECM proteins either by heparin or by plasmin-mediated cleavage of a site within the PlGF-$2_{123–144}$ peptide (*20*).

PlGF-$2_{123–144}$–Abs are retained intratumorally

We examined the tissue retention capacities of PlGF-$2_{123–144}$–Abs. Dense bovine collagen sheet was used as an in vitro tissue-mimicking model and incubated with PlGF-$2_{123–144}$–αPD-L1 or unmodified αPD-L1. After four buffer changes, plasmin digestion released 47.1% of residually bound PlGF-$2_{123–144}$–αPD-L1, whereas <0.1% unmodified αPD-L1 was released, suggesting that PlGF-$2_{123–144}$–αPD-L1 was retained in the collagen matrix (fig. S8). We next performed histological analysis to determine whether PlGF-$2_{123–144}$–Abs remain at the injection site long term after peritumoral injection through binding to endogenous ECM molecules in vivo. Both PlGF-$2_{123–144}$–αCTLA4 and PlGF-$2_{123–144}$–αPD-L1 were detected within the tumor tissue 6 days after injection. In comparison, both unmodified αCTLA4 and unmodified αPD-L1 were not detected at this time point (fig. S9). Together, PlGF-$2_{123–144}$ conjugation enhanced tumor tissue retention of both αCTLA4 and αPD-L1 when injected peritumorally.

PlGF-$2_{123–144}$ conjugation decreases treatment-related adverse events

Because PlGF-$2_{123–144}$–Abs displayed prolonged retention near the injection site, we hypothesized that the concentrations of Abs in plasma would be lower compared to unmodified Abs. To test this hypothesis, we measured the Ab concentrations in blood plasma over time (Fig. 2, A and B). After inoculation with B16F10 cells, mice were given a single administration (100 μg each) of αCTLA4 and αPD-L1 on day 4. Concentrations were highest in all groups on the first day after injection. Furthermore, injection of unmodified Abs via peritumoral and intraperitoneal administration routes showed similar blood plasma concentrations. The concentrations of both PlGF-$2_{123–144}$–Abs in blood plasma were lower compared to their unmodified forms and were barely detected 3 days after injection, suggesting that PlGF-$2_{123–144}$ conjugation may reduce systemic toxicity of αCTLA4/αPD-L1. Neither unmodified αPD-L1 nor PlGF-$2_{123–144}$–αPD-L1 (rat IgG2b) bound to mFcRn with high affinity, confirming that PlGF-$2_{123–144}$ conjugation did not affect Ab recycling (fig. S10). Next, side effects were examined. αCTLA4 and αPD-L1 were administered 4 and 7 days after tumor inoculation, and then serum cytokine concentrations and the liver damage marker alanine aminotransferase (ALT) were examined. Unmodified Ab administration increased both tumor necrosis factor–α (TNFα) and interferon-γ (IFN-γ) concentrations in serum, whereas PlGF-$2_{123–144}$–Abs did not (Fig. 2, C and D). In addition, unmodified Ab, but not PlGF-$2_{123–144}$–Ab treatment, increased ALT activity in the serum (Fig. 2E). Histologic analysis showed that unmodified Abs induced marked morphological changes and lymphocyte infiltration in the liver (Fig. 2F and fig. S11), whereas tissue structure was relatively maintained after PlGF-$2_{123–144}$–Ab treatment. To further evaluate the reduced systemic toxicity achieved by PlGF-$2_{123–144}$ conjugation, we used nonobese diabetic (NOD) male mice, which develop spontaneous diabetes in low frequency but develop autoimmune diabetes after αPD-L1 administration via αPD-L1 binding to islet cells (*21*). Unmodified αPD-L1 administration induced diabetes in all eight of the 16-week-old NOD male mice by day 6, whereas diabetes incidence with PlGF-$2_{123–144}$–αPD-L1 was 0% on 25 days (Fig. 2G). Together, these results indicate that PlGF-$2_{123–144}$ conjugation decreases systemic toxicity of checkpoint blockade Abs.

PlGF-$2_{123–144}$–Abs suppress growth of B16F10 tumors compared to unmodified Abs

We examined the antitumor activity of PlGF-$2_{123–144}$–αCTLA4 + PlGF-$2_{123–144}$–αPD-L1 combination therapy. Four days after ovalbumin (OVA)–expressing B16F10 cell inoculation, αCTLA4 + αPD-L1 (25 μg each per injection) were administered every 3 days for three doses. Neither intraperitoneal nor peritumoral injections of unmodified Abs exhibited antitumor effects at this dose and treatment regimen. In contrast, peritumoral administration of PlGF-$2_{123–144}$–αCTLA4 + PlGF-$2_{123–144}$–αPD-L1 displayed a therapeutic effect, slowing tumor growth and prolonging survival (Fig. 3A and fig. S12A). Administration of αCTLA4 + αPD-L1 + PlGF-$2_{123–144}$ peptide (without conjugation) did not produce an antitumor effect, indicating that the conjugation of PlGF-$2_{123–144}$ to Abs is indispensable for this action.

We repeated administration of both Abs using mice inoculated with wild-type (WT) B16F10 cells lacking the OVA transgene. PlGF-$2_{123–144}$–combination Abs again slowed tumor progression and extended survival, whereas unmodified Abs did not (Fig. 3B and fig. S12B). Higher doses (100 μg each per injection) of PlGF-$2_{123–144}$–Abs using αCTLA4 clone 9H10, which induces T_{reg} depletion (*5*), further suppressed tumor growth and extended survival (Fig. 3C and fig. S12C). Even a single peritumoral injection of PlGF-$2_{123–144}$–combination Abs at a later time point, 7 days after inoculation, with a larger starting tumor volume of 90 mm^3, resulted in smaller tumor size (Fig. 3D and fig. S12D). Further increasing the dose (300 μg each, twice, and then 100 μg each, twice) again slowed tumor growth in the PlGF-$2_{123–144}$–Ab–treated group (Fig. 3E and fig. S12E). All single-agent treatments with PlGF-$2_{123–144}$–αCTLA4 or unmodified αCTLA4 or αPD-L1 exhibited similar growth curves as phosphate-buffered saline (PBS) treatment controls (fig. S13), suggesting that the combination of PlGF-$2_{123–144}$–αCTLA4 and PlGF-$2_{123–144}$–αPD-L1 administration is crucial under these conditions. The PlGF-$2_{123–144}$ peptide did not affect tumor growth in vitro, suggesting that the PlGF-$2_{123–144}$ peptide itself had little effect on tumor growth (fig. S14). Together, these data indicate that local treatment with PlGF-$2_{123–144}$–αCTLA4 + PlGF-$2_{123–144}$–αPD-L1 mediates robust antitumor effects compared to their unmodified forms.

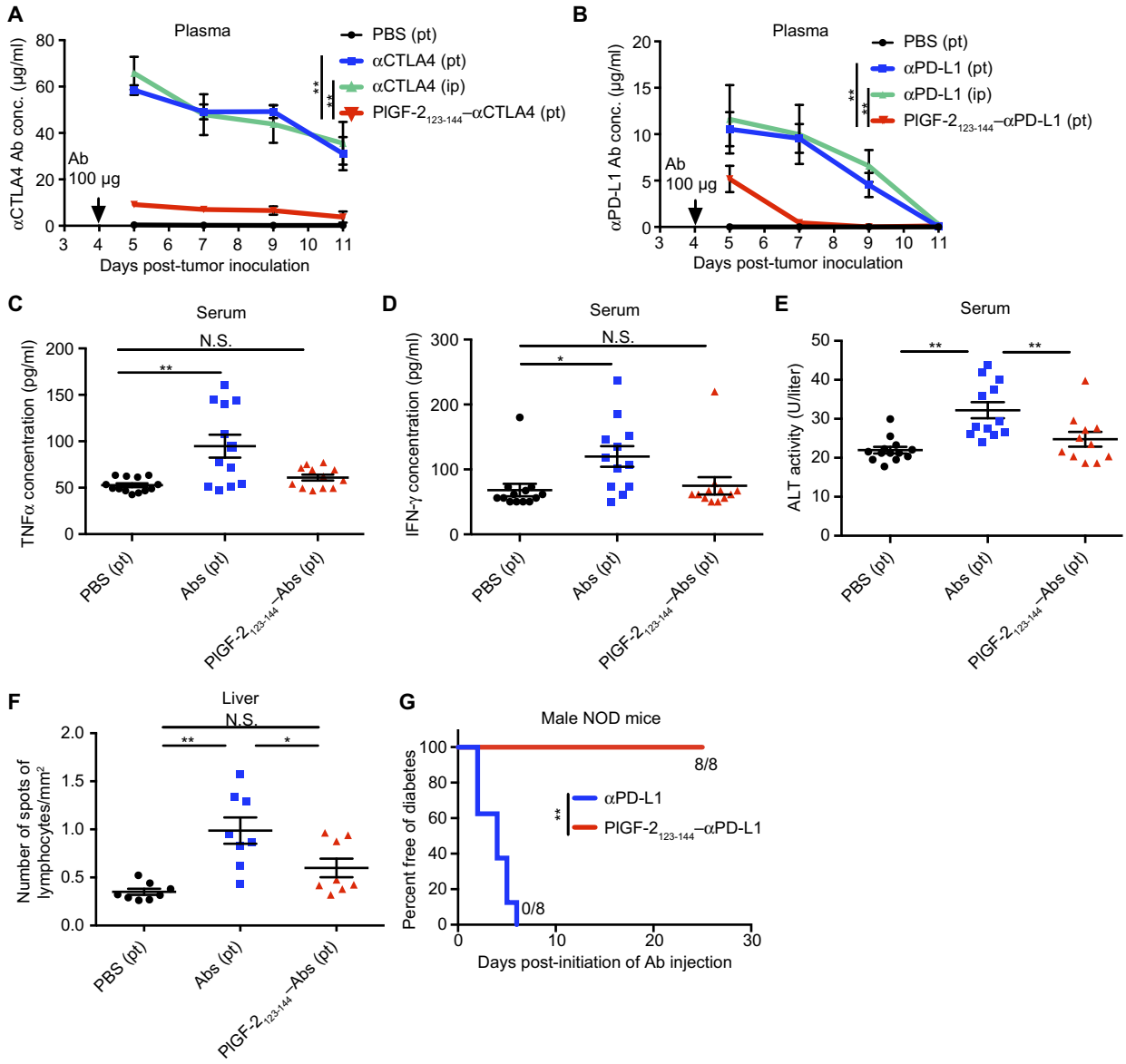

Fig. 2. PlGF-$2_{123–144}$ conjugation reduces systemic exposure to checkpoint blockade Abs and potential treatment-related toxicity. Mice were inoculated with 5×10^5 B16F10 cells on day 0. (**A** and **B**) PlGF-$2_{123–144}$–αCTLA4 and PlGF-$2_{123–144}$–αPD-L1 (100 μg each), αCTLA4 and αPD-L1 (100 μg each), or PBS was administered on day 4. PlGF-$2_{123–144}$–Abs and PBS were injected peritumorally (pt), and unmodified Abs were injected either intraperitoneally (ip) or peritumorally. Blood plasma was collected on days 5, 7, 9, and 11. Concentrations of (A) αCTLA4 and (B) PD-L1 in blood plasma were determined by ELISA [PBS, $n = 6$; Abs (intraperitoneally), $n = 5$; others, $n = 8$; mean ± SEM]. (**C** to **F**) PlGF-$2_{123–144}$–αCTLA4 or unmodified αCTLA4 and αPD-L1 (500 μg each per injection) were injected peritumorally on days 4 and 7. On day 9, blood serum was collected, and concentrations of (C) TNFα and (D) IFN-γ and (E) ALT activity in serum were measured (mean ± SEM). (F) Histologic liver sections were obtained on day 8. The number of lymphocytic infiltration spots was counted and divided by area (mean ± SEM). (**G**) Sixteen-week-old male NOD mice were given 100 μg of PlGF-$2_{123–144}$–αPD-L1 or unmodified αPD-L1 on days 0 and 2 and evaluated for the development of diabetes. All Ab injections were intradermal at the back skin. Clinical diabetes was defined as blood glucose concentrations of 250 mg/dl for three consecutive days. Statistical analyses were done using ANOVA with Tukey's test. Kruskal-Wallis test followed by Dunn's multiple comparison was used in (C) due to nonparametric data. Log-rank (Mantel-Cox) test was performed for diabetes-free survival curves. Two experimental repeats. *$P < 0.05$, **$P < 0.01$. N.S., not significant.

The numbers of activated tumor-infiltrating $CD4^+$ and $CD8^+$ T cells are increased by PlGF-$2_{123–144}$–αCTLA4 + PlGF-$2_{123–144}$–αPD-L1 treatment

To determine the mechanism behind the therapeutic action of PlGF-$2_{123–144}$–combination Ab treatment, we characterized T cell responses in WT B16F10 tumor-bearing mice. Abs were injected twice peritumorally or intraperitoneally, on days 4 and 7 after tumor inoculation. On day 8, leukocytes were extracted from the tumor, tumor-draining lymph node (tdLN), and spleen. PlGF-$2_{123–144}$–combination Abs increased the number and frequency of $CD8^+CD3^+$ T cells within the tumor compared to unmodified Abs and PBS injections (Fig. 4, A and B). The percentages of the effector population (defined as $CD62L^-CD44^+$) and PD-1^+CD8^+ T cells were increased compared to PBS treatment, indicating activation of $CD8^+$ T cells (Fig. 4, C and

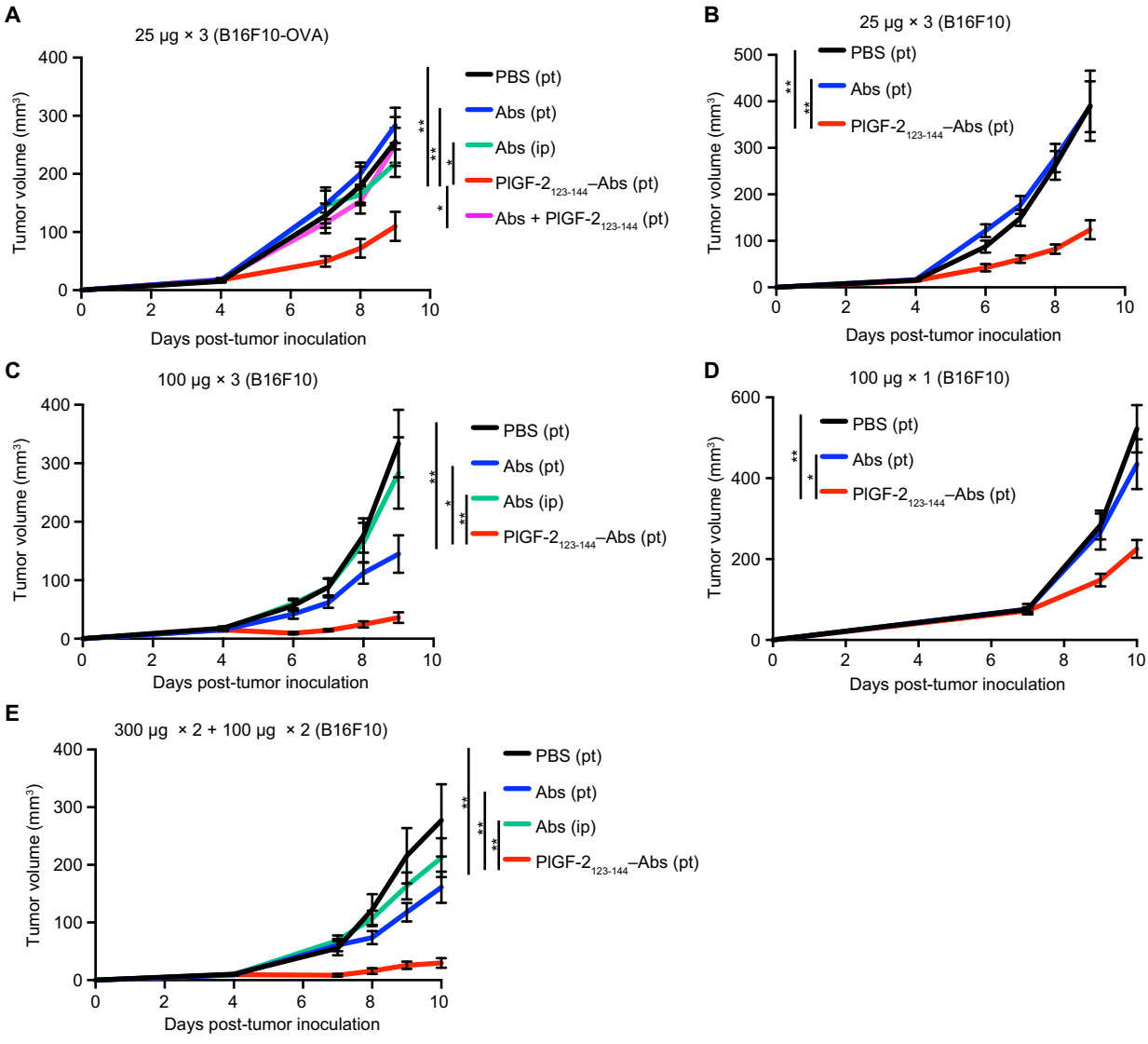

Fig. 3. PlGF-$2_{123-144}$–αCTLA4 + PlGF-$2_{123-144}$–αPD-L1 treatment reduces B16F10 melanoma growth rate. (**A**) B16F10-OVA cells (1×10^6) or (**B** to **E**) B16F10 cells (5×10^5) were inoculated on day 0. PlGF-$2_{123-144}$–αCTLA4 + PlGF-$2_{123-144}$–αPD-L1 (PlGF-$2_{123-144}$–Abs), αCTLA4 + αPD-L1 (Abs), Abs + non–cross-linked PlGF-$2_{123-144}$ peptide, or PBS was administered (A and B) 25 μg on days 4, 7, and 10; (C) 100 μg on days 4, 7, and 10; (D) 100 μg on day 7; or (E) 300 μg on days 4 and 6, and 100 μg on days 9 and 12. Abs were injected either intraperitoneally or peritumorally. Ab doses per administration are indicated in the figure. αCTLA4 clones 4F10 (A and B) and 9H10 (C to E) were used. Graphs depict tumor volume until the first mouse died. Tumor volumes are presented as means ± SEM. (A) PBS (peritumorally), $n = 10$; Abs (peritumorally), $n = 8$; Abs (intraperitoneally), $n = 7$; PlGF-$2_{123-144}$–Abs (peritumorally), $n = 12$; Abs + PlGF-$2_{123-144}$ (peritumorally), $n = 8$. (B) Abs (peritumorally), $n = 7$; other treatment groups, $n = 9$. (C) $n = 10$. (D) PlGF-$2_{123-144}$–Abs (peritumorally), $n = 8$; other treatment groups, $n = 7$. (E) Abs (intraperitoneally), $n = 6$; PlGF-$2_{123-144}$–Abs (peritumorally), $n = 8$; other treatment groups, $n = 7$. Three experimental repeats. Statistical analyses were done using ANOVA with Tukey's test. *$P < 0.05$, **$P < 0.01$.

D). PlGF-$2_{123-144}$–combination Abs also increased the number of $CD4^+$ T cells in the tumor (Fig. 4, E and F). The percentage of effector $CD4^+$ T cells was increased as well (Fig. 4G) (*22*, *23*). The percentage of $CD25^+Foxp3^+$ T_{regs} in the $CD4^+$ T cell population was maintained (Fig. 4H).

To test whether tumor-infiltrating $CD8^+$ T cells produced more effector cytokines and higher levels of cytotoxicity, $CD8^+$ T cells were extracted and stimulated ex vivo using αCD3 and αCD28 (*13*). The PlGF-$2_{123-144}$–combination Abs increased the percentage of granzyme B^+ ($Gzmb^+$), interleukin-2^+ ($IL\text{-}2^+$), $TNF\alpha^+$, and IFN-γ^+ cells in $CD8^+$ tumor-infiltrating T cells compared to the PBS control group (Fig. 4, I to L). PlGF-$2_{123-144}$–combination Abs did not affect the percentages of T_{regs} and effector $CD8^+$ T cells in the tdLN and spleen, whereas central memory and PD-1^+CD8^+ T cells were increased (Fig. 4, M to P, and fig. S15). This result suggests that these PlGF-$2_{123-144}$–Ab treatments increased tumor antigen–experienced T cells systemically. Finally, PlGF-$2_{123-144}$–combination Ab treatment increased $OVA_{257-264}$ antigen-specific $CD8^+$ T cells in the tdLN, tested in the B16F10-OVA model (fig. S16). Collectively, PlGF-$2_{123-144}$–αCTLA4 + PlGF-$2_{123-144}$–αPD-L1 treatment effectively activated tumor-infiltrating T cells, resulting in the therapeutic effects observed in Fig. 3.

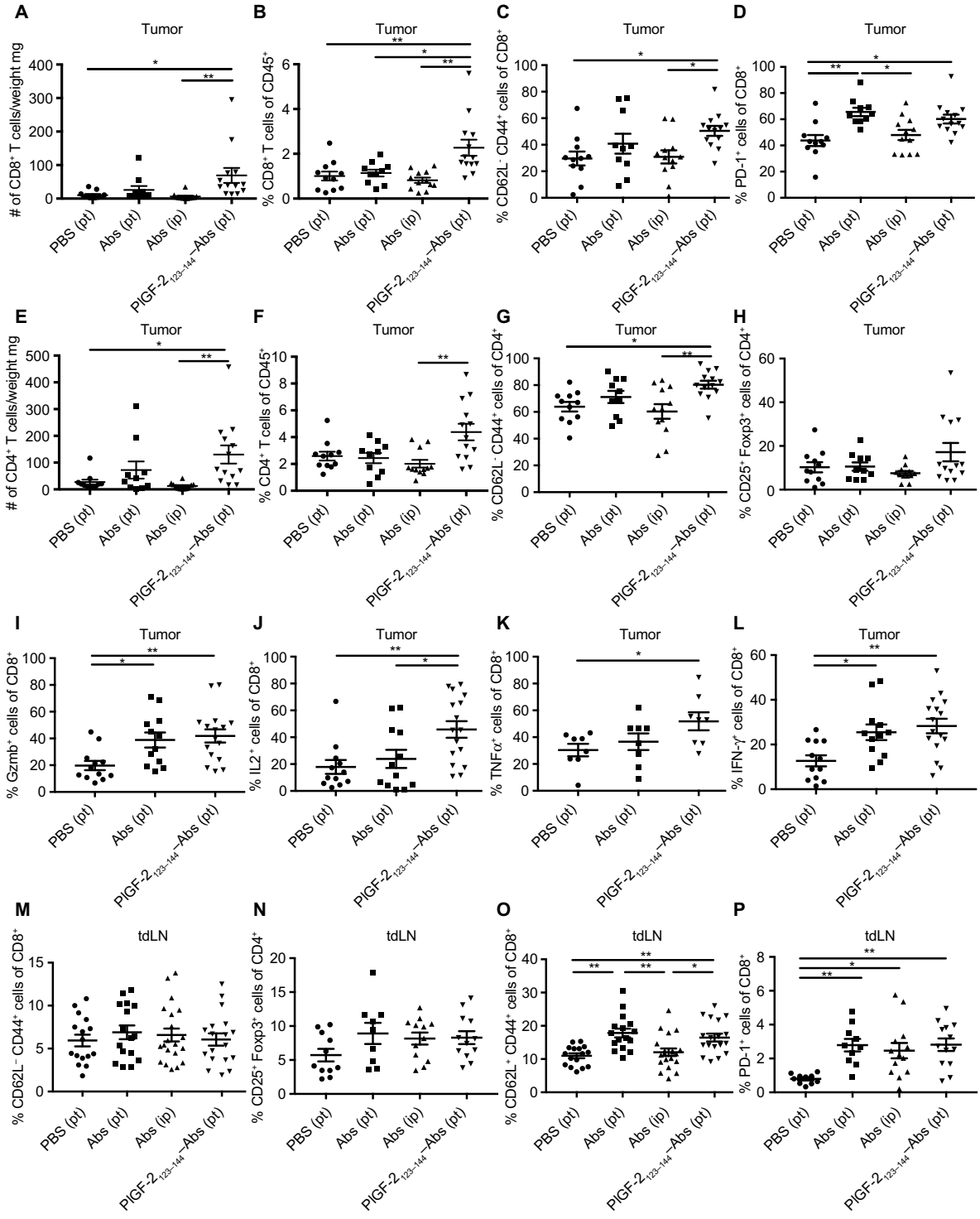

Fig. 4. PlGF-$2_{123–144}$–αCTLA4 + PlGF-$2_{123–144}$–αPD-L1 treatment promotes T cell activation and increases B16F10 melanoma-infiltrating $CD8^+$ T cells. B16F10 cells (5×10^5) were inoculated on day 0. PlGF-$2_{123–144}$–αCTLA4 + PlGF-$2_{123–144}$–αPD-L1 (PlGF-$2_{123–144}$–Abs), αCTLA4 + αPD-L1 (Abs), or PBS was administered on days 4 and 7. Abs were injected at 100 μg of each per injection either intraperitoneally or peritumorally. Clone 9H10 was used as αCTLA4. Tumor and tdLN were collected on day 8 and analyzed by flow cytometry. (**A**) Number and (**B**) frequency of $CD8^+CD3^+$ tumor-infiltrating T cells. (**C**) Frequencies of $CD62L^-CD44^+$ effector cells and (**D**) $PD\text{-}1^+$ cells among $CD8^+CD3^+$ tumor-infiltrating T cells. (**E**) Number and (**F**) frequency of $CD4^+CD3^+$ tumor-infiltrating T cells. (**G**) Frequencies of $CD62L^-CD44^+$ effector cells and (**H**) $CD25^+Foxp3^+$ T_{regs} among $CD4^+CD3^+$ tumor-infiltrating T cells. (**I** to **L**) T cells were extracted from tumors and stimulated with αCD28 and αCD3 for 6 hours. Graphs depict the % of (I) $Gzmb^+$, (J) $IL\text{-}2^+$, (K) $TNF\alpha^+$, and (L) $IFN\text{-}\gamma^+$ cells among $CD8^+CD3^+$ T cells. (**M** to **P**) Graphs depict the % of (M) $CD62L^-CD44^+$ effector cells of $CD8^+CD3^+$ T cells, (N) $CD25^+Foxp3^+$ T_{regs} of $CD4^+CD3^+$ T cells, (O) $CD62L^+CD44^+$ memory, and (P) $PD\text{-}1^+$ cells among $CD8^+CD3^+$ T cells in tdLN. Two experimental repeats. Statistical analyses were done using ANOVA with Tukey's test. Kruskal-Wallis test followed by Dunn's multiple comparison was used in (E), (F), and (P) due to nonparametric data. $^*P < 0.05$, $^{**}P < 0.01$.

PlGF-$2_{123-144}$–Ab treatment induces systemic antitumor immunity

The increase of systemic central memory and PD-$1^{+}CD8^{+}$ T cells, as well as stimuli-responsive cytokine-producing $CD8^{+}$ T cells in the tumor after PlGF-$2_{123-144}$–αCTLA4 + PlGF-$2_{123-144}$–αPD-L1 treatment, led us to investigate whether PlGF-$2_{123-144}$–Abs could mediate antitumor responses in a distant tumor. B16F10 cells were inoculated in the left back of the mouse on day 0 and in the right back of the mouse on day 2 (Fig. 5A). Subsequently, the Abs were injected peritumorally beside the left tumor or intraperitoneally on days 4, 7, and 10. The peritumoral injection of PlGF-$2_{123-144}$–combination Abs slowed the outgrowth of both the left (ipsilateral) and right (contralateral) tumors (Fig. 5, B and C, and fig. S17). In contrast, unmodified Abs had little therapeutic effect on either tumor when injected peritumorally or intraperitoneally. These data indicate that PlGF-$2_{123-144}$–αCTLA4 + PlGF-$2_{123-144}$–αPD-L1 treatment near one tumor enhances a systemic antitumor immunological activity.

PlGF-$2_{123-144}$–Ab treatment has therapeutic effects on genetically engineered mouse models of melanoma and breast cancer

To extend our results beyond transplantable tumor models, we used *Tyr:Cre-ER*$^{+}$*/LSL-Braf*^{V600E}*/Pten*$^{fl/fl}$ mice, which are engineered with Cre-inducible expression of active *Braf* and biallelic deletion of *Pten*, commonly altered molecular pathways in human melanoma (*24*). After tumor induction via local application of 4-OH-tamoxifen, PlGF-$2_{123-144}$–αCTLA4 + PlGF-$2_{123-144}$–αPD-L1 was administered via peritumoral injection. The matrix-binding Abs markedly reduced tumor growth compared to PBS-treated or unmodified Ab–treated groups (Fig. 6A). We similarly investigated the MMTV-PyMT (mouse mammary tumor virus–polyomavirus middle T antigen) model of breast cancer (*25*) and found that peritumoral administration of the PlGF-$2_{123-144}$–combination Abs also suppressed tumor growth and prolonged survival in these mice (Fig. 6, B and C). PlGF-$2_{123-144}$–combination Ab administration induced eradication of tumors in 11 of 16 mice, whereas combination treatment with unmodified Abs eradicated tumors in 5 of 15 mice. To assess long-term anticancer immune protection, mice whose tumors were eradicated by PlGF-$2_{123-144}$–combination Ab treatment were rechallenged with MMTV-PyMT cells. Only one of these nine mice developed palpable tumors, whereas all naïve mice grew detectable tumors, suggesting that PlGF-$2_{123-144}$–combination Abs induced immunologic memory (Fig. 6D). These data indicate that the PlGF-$2_{123-144}$–αCTLA4 + PlGF-$2_{123-144}$–αPD-L1 therapeutic effect is applicable to multiple cancer types.

DISCUSSION

Recently, αCTLA4 and αPD-1/αPD-L1 monoclonal Abs have been recognized as highly promising drugs for cancer treatment, exhibiting therapeutic effects on various types of cancer (*12*, *26*–*28*). Although their therapeutic effects in the clinic are remarkable, treatment-related adverse events are serious problems (*14*, *29*, *30*). Here, the incidence of such adverse events due to checkpoint blockade was reduced by PlGF-$2_{123-144}$ conjugation with peritumoral administration. PlGF-$2_{123-144}$–Abs, which remain localized near the tumor tissue injection site and thus reduce the concentration in the blood circulation, may maintain the systemic immune homeostasis by avoiding influence on non–tumor

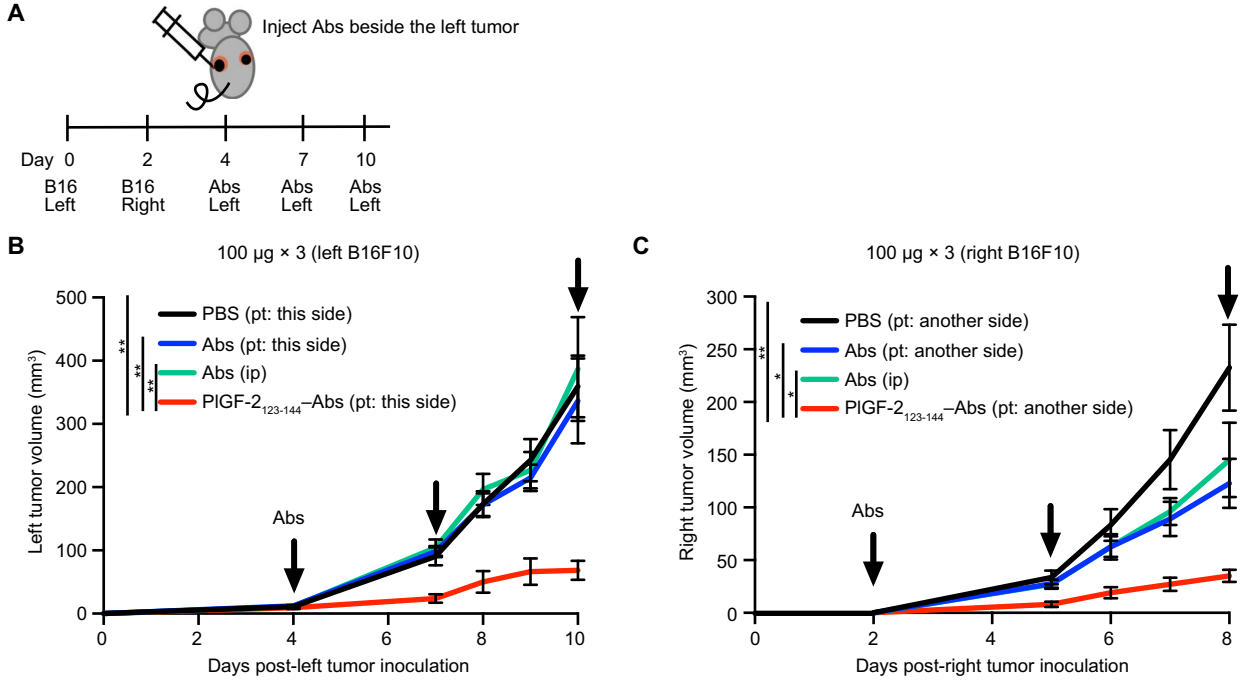

Fig. 5. PlGF-$2_{123-144}$–αCTLA4 + PlGF-$2_{123-144}$–αPD-L1 treatment induces systemic antitumor immunity. (**A**) Schedule of tumor inoculation and Ab administration throughout the experiment. B16F10 cells (5×10^5) were inoculated intradermally on day 0 in the left side of mouse back skin and then repeated on day 2 in the right side. PlGF-$2_{123-144}$–αCTLA4 + PlGF-$2_{123-144}$–αPD-L1 (PlGF-$2_{123-144}$–Abs), αCTLA4 + αPD-L1 (Abs), or PBS was administered on days 4, 7, and 10. Abs were injected at 100 μg of each per injection either intraperitoneally or peritumorally. Peritumoral injections were performed only beside the left tumor, but not the right tumor. (**B**) Tumor volumes of the tumor on the left back and (**C**) the tumor on the right back were measured ($n = 9$, mean ± SEM). Two experimental repeats. Statistical analyses were done using ANOVA with Tukey's test. *$P < 0.05$, **$P < 0.01$.

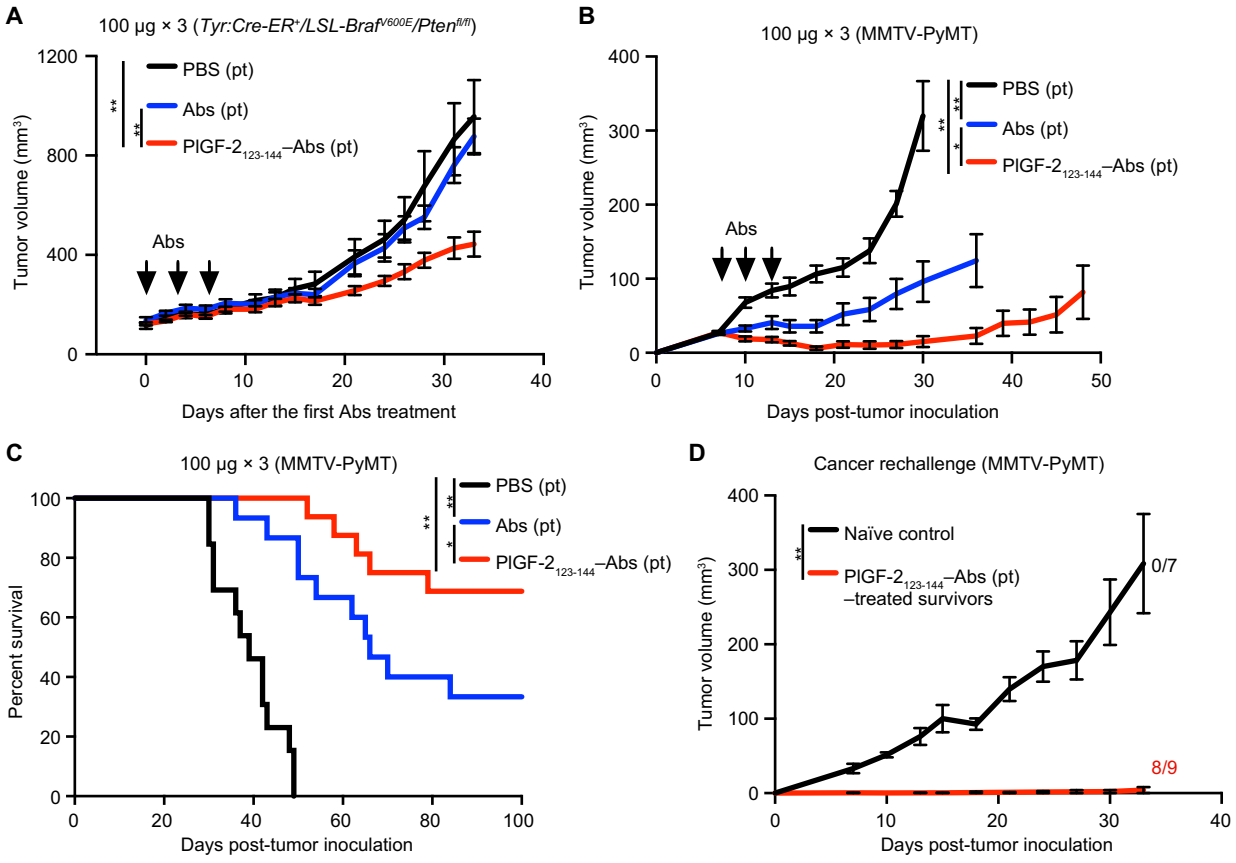

Fig. 6. PlGF-$2_{123–144}$–αCTLA4 + PlGF-$2_{123–144}$–αPD-L1 treatment exhibits antitumor activity in clinically relevant cancer models. (**A**) *Tyr:Cre-ER*$^{+}$*/LSL-Braf*^{V600E}*/Pten*$^{fl/fl}$ mice received 50 μg of 4-OH-tamoxifen on their back skin to induce melanoma development. Day 0 is defined as the time point when tumors first become visible. PlGF-$2_{123–144}$–αCTLA4 + PlGF-$2_{123–144}$–αPD-L1 (PlGF-$2_{123–144}$–Abs), αCTLA4 + αPD-L1 (Abs), or PBS was injected peritumorally on days 0, 3, and 6. Abs were injected at 100 μg of each per injection. (**B** and **C**) MMTV-PyMT cells were obtained from spontaneously developed breast cancer in FVB-Tg(MMTV-PyVT) transgenic mice and cultured in vitro. MMTV-PyMT cells (8×10^5) were inoculated into the right mammary gland fat pad. After 7, 10, and 13 days, Abs were injected at 100 μg of each per injection peritumorally. (**D**) Thirty days after the first tumor inoculation, MMTV-PyMT cells (8×10^5) were again inoculated into the left mammary gland fat pad in PlGF-$2_{123–144}$–Ab–treated tumor-free survivors or in naïve mice. Numbers indicate how many mice remain tumor-free among total mice at the end of the experiment. Graphs depict (A, B, and D) tumor volume until the first mouse died and (C) survival rates. αCTLA4 clone 9H10 was used. Tumor volumes are presented as means ± SEM. (A) PBS (peritumorally), $n = 9$; Abs (peritumorally), $n = 11$; PlGF-$2_{123–144}$–Abs (peritumorally), $n = 12$. (B and C) PBS (peritumorally), $n = 13$; Abs (peritumorally), $n = 15$; PlGF-$2_{123–144}$–Abs (peritumorally), $n = 16$. (D) Naïve, $n = 7$; survivors, $n = 9$. Three experimental repeats. Statistical analyses were done using ANOVA with Tukey's test. Kruskal-Wallis test followed by Dunn's multiple comparison was used in (B) due to nonparametric data. For single comparisons, a two-tailed Student's *t* test was used. Log-rank (Mantel-Cox) test for survival curves. $^*P < 0.05$, $^{**}P < 0.01$.

antigen–specific T cells. In the NOD mouse model, we showed that PlGF-$2_{123–144}$ conjugation reduces the risk of PD-L1/PD-1 inhibition-induced autoimmune diabetes, which has been reported in the clinic (*31*–*33*). We assume that the reason why none of the NOD mice developed diabetes during 25 days after PlGF-$2_{123–144}$–αPD-L1 injections is that PlGF-$2_{123–144}$–αPD-L1 is barely detected in the blood plasma 3 days after injections. PlGF-$2_{123–144}$ conjugation may even allow decreases in the administered dose because we observed tumor growth delay at low dosages, where unmodified Abs had no effect. These data are encouraging with regard to treatment of patients who have discontinued checkpoint blockade therapy due to adverse events, as well as those who are not amenable to systemic chemotherapy.

Local immune therapy has been reported to have equivalent antitumor efficacy to systemic administration of therapeutics through efficient activation of immune systems (*34*–*39*). Recently, intratumoral administration of cytokines, adjuvants, genes, dendritic cells, and immunomodulatory Abs has been tested in the clinic (*40*). Regarding checkpoint blockade, clinical trials have been performed with intratumoral injection of αCTLA4 (ipilimumab) in melanoma, colorectal cancer, and lymphoma (*40*). Intratumoral injection with the combination of ipilimumab and IL-2 generated responses in both injected and noninjected lesions in the majority of patients in a phase 1 clinical trial (*41*). In a mouse model, local administration of αCTLA4 with slow-release formulations (such as Montanide oil emulsion or polymer microparticles) enabled the use of lower doses of Ab while maintaining antitumor efficacy (*34*, *36*, *37*). In our study, we have developed a molecular engineering approach to provide for local checkpoint blockade and enable injection site retention without biomaterial carriers, which resulted in enhanced antitumor efficacy and reduced adverse events compared to local injection of the unmodified forms of checkpoint blockade. Because PlGF-$2_{123–144}$–Abs promiscuously bind to ECM proteins, as shown above, their enhanced antitumor efficacy should be primarily observed when they are injected locally.

Growth of B16F10 and *Tyr:Cre-ER*$^+$*/LSL-Braf*^{V600E}*/Pten*$^{fl/fl}$ melanomas was difficult to slow using conventional αCTLA4 and αPD-L1 therapy under our experimental conditions, even when locally administered. In contrast, local antitumor activity with PlGF-$2_{123–144}$–αCTLA4 + PlGF-$2_{123–144}$–αPD-L1 substantially delayed growth of these melanomas. Because PlGF-$2_{123–144}$ itself does not bind to the vascular endothelial growth factor receptor (*20*) and did not affect tumor growth in vitro or in vivo, retention and local release should markedly improve the therapeutic effect of αCTLA4 and αPD-L1 through efficient activation of endogenous T cells. However, the PlGF-$2_{123–144}$–combination Abs did not fully eradicate B16F10 and *Tyr:Cre-ER*$^+$*/LSL-Braf*^{V600E}*/Pten*$^{fl/fl}$ melanoma in all mice. To accomplish complete eradication of immunosuppressed tumors, PlGF-$2_{123–144}$–αCTLA4 + PlGF-$2_{123–144}$–αPD-L1 in combination with other therapies (*42*–*44*) may be necessary. As for the MMTV-PyMT breast cancer model, PlGF-$2_{123–144}$–combination Abs eradicated cancers in 69% of mice compared to 33% in the unmodified Ab–treated controls. These data suggest that PlGF-$2_{123–144}$–αCTLA4 + PlGF-$2_{123–144}$–αPD-L1 effectively suppresses growth of multiple cancer types, but complete remission is dependent on the type of cancer.

Our localized therapy also suppressed growth of a tumor contralateral to the injection site, which is consistent with earlier observations of induction of systemic immunity (*35*, *36*, *38*, *39*). These data suggest that it may be feasible to treat patients with oligometastatic tumors by PlGF-$2_{123–144}$–αCTLA4 + PlGF-$2_{123–144}$–αPD-L1 treatment. With the low concentration of PlGF-$2_{123–144}$–conjugated Abs in the blood combined with the increase in activated CD8$^+$ T cells, the mechanism of distant tumor treatment is likely due to effective tumor antigen–specific CD8$^+$ T cell activation, which is disseminated systemically. Unmodified Abs distributed systemically via intraperitoneal or peritumoral administration did not suppress B16F10 tumor growth at the doses used in this study. Peritumoral injections of unmodified Abs resulted in increased Gzmb$^+$ and IFN-γ$^+$ CD8$^+$ T cells in tumors, as well as increased central memory and PD-1$^+$CD8$^+$ T cells in the tdLN. However, the numbers of tumor-infiltrating CD8$^+$ and CD4$^+$ T cells did not increase compared to PBS treatment. In addition, the percentage of CD8$^+$ T cells producing an IL-2 in response to stimulation was higher for PlGF-$2_{123–144}$–conjugated Abs compared to unmodified Abs. Because IL-2$^+$CD8$^+$ T cells play a crucial role in antitumor immune responses (*13*, *43*, *45*), that may explain why peritumoral injection of PlGF-$2_{123–144}$–αCTLA4 + PlGF-$2_{123–144}$–αPD-L1, but not unmodified Abs, suppressed tumor outgrowth in both ipsilateral and contralateral tumors.

By design, PlGF-$2_{123–144}$–IgG binds to a variety of ECM proteins, which should contribute to prolonged tissue retention at the injection site, as we have previously seen in PlGF-$2_{123–144}$–fused GFs (*20*). Bound PlGF-$2_{123–144}$–Abs can be released by plasmin. Because cancer cells secrete more proteases than normal cells (*46*, *47*), cancer-derived proteases may contribute to PlGF-$2_{123–144}$–Ab release from ECM in vivo.

We used two αCTLA4 clones (9H10 and 4F10) to investigate whether T_{reg} depletion contributes to antitumor efficacy. Because both clones suppressed tumor growth in their PlGF-$2_{123–144}$–conjugated forms, it appears that αCTLA4 primarily contributed to the antitumor activity through its effect of ligand blocking rather than T_{reg} depletion.

From the point of view of clinical translation, a major advantage of PlGF-$2_{123–144}$–checkpoint blockade is material availability. Checkpoint blockade Abs are already used in the clinic, and PlGF-$2_{123–144}$ peptide, which is derived from the human sequence, is short enough to be chemically synthesized on a large scale with nonbiological origin. Moreover, synthesizing PlGF-$2_{123–144}$–Abs is simple. Reactions can be performed under aqueous conditions in only 90 min, using chemistry that is analogous to PEGylation of proteins. These features may help PlGF-$2_{123–144}$–checkpoint blockade to overcome the barriers to clinical translation. A limitation of synthesizing PlGF-$2_{123–144}$–Abs is the inability to control the site of peptide conjugation. However, we have shown that PlGF-$2_{123–144}$ conjugation did not alter the Ab-antigen affinities. The same reaction is also used to make antibody-drug conjugates, such as trastuzumab emtansine (*48*).

In conclusion, we found that the antitumor activity of αCTLA4 and αPD-L1 was enhanced by the addition of ECM-binding properties. Conjugation of PlGF-$2_{123–144}$ enhanced injection site tissue retention of the conjugated Abs. A clear reduction in systemic side effects, including autoimmunity, was demonstrated in association with lower Ab concentrations in plasma. Peritumoral injections of PlGF-$2_{123–144}$–αCTLA4 + PlGF-$2_{123–144}$–αPD-L1 activated tumor-infiltrating T cells, resulting in delayed tumor growth and prolonged survival, and suppressing growth in a distant tumor and in a tumor rechallenge model as well. This simple approach of engineering ECM-binding Abs may hold potential for clinical translation of immune checkpoint blockade for localized delivery as a cancer therapeutic.

MATERIALS AND METHODS

Study design

This study was designed to test the antitumor efficacy and adverse effects of matrix-binding checkpoint blockade Abs against melanoma and breast cancer with local injection compared to conventional checkpoint blockade. We tested whether the local activation of antitumor immune response after matrix-binding checkpoint blockade Ab treatment would suppress the growth of a distant tumor. These experiments were designed to develop therapeutic strategies to improve the conventional form of checkpoint blockade in the clinic. Statistical methods were not used to predetermine necessary sample size, but sample sizes were chosen on the basis of estimates from pilot experiments and previously published results such that appropriate statistical tests could yield significant results. Synthesis of PlGF-$2_{123–144}$–Ab and tumor treatments were performed by multiple individuals to ensure reproducibility. All experiments were replicated at least twice. For animal studies, mice were randomized into treatment groups within a cage immediately before the first Ab injection, and all mice were treated the same way. Tumor growth was determined by direct measurement of the tumors. The survival endpoint was reached when the tumor size reached more than 500 mm^3 for B16F10 melanoma and MMTV-PyMT breast cancer and more than 1000 mm^3 for *Tyr:Cre-ER*$^+$*/LSL-Braf*^{V600E}*/Pten*$^{fl/fl}$ melanoma. The *n* values used to calculate statistics are indicated in the figure legends. Samples were not excluded from analysis. Experiments were not performed in a blinded fashion except for counting liver-infiltrating lymphocytes. Statistical methods are described in the "Statistical analysis" section. Original data are located in table S1.

Synthesis of PlGF-$2_{123–144}$–Abs

Rat anti-mouse PD-L1 (clone 10F.9G2, Bio X Cell), hamster anti-mouse CTLA4 (clone UC10-4F10-11 or 9H10, Bio X Cell), or rat IgG2a control Ab (BioLegend) was incubated with 15 equiv. of sulfo-SMCC for 30 min at room temperature. Excess sulfo-SMCC was removed using a Zeba spin desalting column (Thermo Fisher Scientific). Fifteen equivalents of the PlGF-$2_{123–144}$ peptide (RRRPKGRGKRRREKQRPTDCHL) was then added and reacted for 1 hour at 4°C. Endotoxin concentration was checked by QUANTI-Blue assay (Invivogen) using HEK-Blue

mTLR4 cells (Invivogen), not to exceed 0.1 endotoxin unit per mouse injection limit. The peptide was synthesized with >95% purity by GenScript.

SDS–polyacrylamide gel electrophoresis

SDS-PAGE was performed on 4 to 20% gradient gels (Bio-Rad) after Abs were reduced with 10 mM dithiothreitol. After electrophoresis, gels were stained with SimplyBlue SafeStain (Thermo Fisher Scientific) according to the manufacturer's instruction. Gel images were acquired with the ChemiDoc XRS+ system (Bio-Rad).

Matrix-assisted laser desorption/ionization–time-of-flight mass spectrometry

MALDI-TOF MS analyses were done by the proteomics core facility at the Ecole Polytechnique Fédérale de Lausanne (EPFL). Ab solutions were dialyzed to exchange the buffer to 50 mM ammonium bicarbonate. The Ab samples (5 to 10 μg) were desalted with a C4 filter pipette tip (custom-made 250-μg capacity) and then eluted using 85% acetonitrile, 0.1% trifluoroacetic acid in water. The cleaned Abs were dried in SpeedVac for 10 min and resolubilized in 5 μl of 2% acetonitrile, 0.1% trifluoroacetic acid in water. Analyses by MALDI-TOF were conducted on an Applied Biosystems 4800 MALDI TOF/TOF mass spectrometer using high mass linear positive mode. Typically, spectra from 1000 to 1500 laser shots were summed to obtain the final spectrum. MALDI Matrix 2,5-dihydroxybenzoic acid (Applied Biosystems) at 70 mg/ml in methanol was used for all experiments. Analyte (0.5 μl) and matrix solution (1 μl) were deposited on the stainless steel target, mixed with a micropipette, and allowed to air-dry, forming a cocrystalline sample/matrix complex. The measurements were externally calibrated at three points with a mix of carbonic anhydrase, enolase, and BSA (Sigma-Aldrich).

Nanoparticle tracking analysis

Particle concentration in the unmodified or PlGF-$2_{123–144}$–Ab solution was analyzed with a NanoSight NS300 (Malvern Instruments), equipped with a low volume flow cell gasket and a 532-nm green laser module. The Ab solution was injected manually in the sample chamber with syringes until the solution reached the tip of the nozzle and then infused at a constant flow rate using a syringe pump for measurements. All measurements were performed at room temperature. The software used for capturing and analyzing the data was the NTA 3.2 Dev Build 3.2.16. The samples were measured for 60 s. One thousand four hundred ninety-eight frames were analyzed in each analysis.

Detection of Ab binding to ECM proteins

Ninety-six–well ELISA plates (Greiner Bio-One) were coated with recombinant human ECM proteins (10 μg/ml), fibronectin (Sigma-Aldrich), fibrinogen (von Willebrand factor– and fibronectin-depleted; Enzyme Research Laboratories), osteopontin (Sigma-Aldrich), vitronectin (Sigma-Aldrich), collagen I (EMD Millipore), collagen II (EMD Millipore), collagen III (EMD Millipore), or collagen IV (EMD Millipore) in PBS for 1 hour at 37°C, followed by blocking with 2% BSA in PBS with 0.05% Tween 20 (PBS-T) for 1 hour at room temperature. Then, wells were washed with PBS-T and further incubated with PlGF-$2_{123–144}$–Abs or unmodified Abs (10 μg/ml each) for 1 hour at room temperature. After three washes with PBS-T, wells were incubated for 1 hour at room temperature with horseradish peroxidase (HRP)–conjugated Abs against rat IgG or hamster IgG (Jackson ImmunoResearch). After washes, bound Abs were detected with tetramethylbenzidine substrate by measurement of the absorbance at 450 nm with subtraction of the absorbance at 570 nm.

Binding affinity assay

Ninety-six–well ELISA plates (Greiner Bio-One) were coated with fibronectin, collagen I, rmCTLA4 (Sino Biological), or rmPD-L1 (Sino Biological) (10 μg/ml each; in PBS) for 1 hour at 37°C, followed by blocking with 2% BSA in PBS-T for 1 hour at room temperature. Then, wells were washed with PBS-T and further incubated with PlGF-$2_{123–144}$ or unmodified Abs at increasing concentrations for 1 hour at room temperature. After three washes with PBS-T, wells were incubated for 1 hour at room temperature with HRP-conjugated Abs against hamster IgG or rat IgG. After washes, bound Abs were detected with tetramethylbenzidine substrate by measurement of the absorbance at 450 nm with subtraction of the absorbance at 570 nm. The apparent K_d values were obtained by nonlinear regression analysis in Prism software (version 7, GraphPad Software) assuming one-site–specific binding.

Inhibition of PlGF-$2_{123–144}$–Ab binding to fibronectin by heparin

Ninety-six–well ELISA plates were coated with fibronectin (10 μg/ml) in PBS for 1 hour at 37°C and further blocked with 2% BSA in PBS-T for 1 hour at room temperature. Then, wells were washed with PBS-T and incubated with PlGF-$2_{123–144}$–conjugated rat IgG2a control Ab (10 μg/ml; in PBS-T with 0.1% BSA) with increasing concentrations of heparin for 1 hour at room temperature. After three washes with PBS-T, bound Abs were detected using HRP-conjugated goat anti-rat secondary Ab (Jackson ImmunoResearch).

PlGF-$2_{123–144}$ cleavage by plasmin

PlGF-$2_{123–144}$–Abs (1 mg/ml) were incubated with plasmin (0.1 U/ml) overnight at 37°C. Cleavage of PlGF-$2_{123–144}$ by plasmin was detected by SDS-PAGE. ECM-binding affinity of plasmin-treated Ab was determined by ELISA as described above.

Release profiles of PlGF-$2_{123–144}$–αPD-L1 and αPD-L1 from collagen gels

Collagen gels were prepared by mixing 8.5 ml of bovine collagen (5 mg/ml; Symatese) with 800 μl of 10× MEM (Life Technologies) followed by 1.8 ml of NaOH (0.1 M). Five hundred microliters of neutralized collagen solution was allowed to gel in 1.5-ml protein low-binding tubes (Thermo Fisher Scientific). After 15 min of gelation, PlGF-$2_{123–144}$–αPD-L1 or αPD-L1 (10 μg/ml) was incubated for 3 hours in 800 μl of release buffer (0.1% BSA in PBS), followed by wash with release buffer. Thereafter, 800 μl of release buffer was added to each collagen gel and incubated at 37°C (5% CO_2). Every 24 hours, release buffer aliquots were taken and frozen down, followed by the addition of new release buffer to the collagen gels. These release buffer steps were repeated five times. After the fifth buffer change, the collagen gels were incubated with plasmin for 12 hours (0.1 U/ml; Roche). To get the release profile of the Abs from collagen gel, all the collected release samples were thawed, and the concentrations were obtained by ELISA as described above.

Mice and cell lines

C57BL/6 and FVB mice, ages 8 to 12 weeks, were obtained from Charles River, unless otherwise noted. NOD mice were obtained from The Jackson Laboratory and bred in the animal facility at the University of Chicago. *Tyr:Cre-ER$^+$/LSL-Braf^{V600E}/Pten$^{fl/fl}$* mice, ages 6 to 12 weeks, were

provided by T. Gajewski (University of Chicago). Experiments were performed with the approval from the Veterinary Authority of the Canton de Vaud, Switzerland, and the Institutional Animal Care and Use Committee of the University of Chicago. B16F10 and B16F10-OVA cells were obtained from the American Type Culture Collection and cultured according to the instructions. MMTV-PyMT cells were obtained from spontaneously developed breast cancer in FVB-Tg (MMTV-PyVT) transgenic mice (polyoma middle T antigen oncogene expression was induced by mouse mammary tumor virus promotor) and cultured in vitro. All cell lines were checked for mycoplasma contamination by an IMPACT I pathogen test (IDEXX BioResearch).

Abs retention analysis and immunohistochemistry of skin tissue sections

The backs of C57BL/6 mice were shaved. A total of 5×10^5 B16F10 cells resuspended in 50 μl of PBS were injected intradermally on the left side of the back of each mouse. After 4 days, mice were injected with 10 μg of αCTLA4 (4F10) and αPD-L1 (peritumorally). Histological analysis was performed on serial sections (10-μm frozen sections) until reaching the central portion of the melanoma. Cryosections, fixed with 4% paraformaldehyde (PFA) and blocked with 2% BSA, were incubated with Alexa Fluor 488–conjugated anti-hamster or anti-rat Ab (both from Jackson ImmunoResearch) and biotinylated anti-S100 Ab (Invitrogen) for 1 hour at room temperature, followed by staining with Alexa Fluor 647–conjugated streptavidin (BioLegend). Images were taken with DMi8 microscope (Leica).

Ab concentration analysis

B16F10 melanoma cells (5×10^5) were injected intradermally on the left side of the back of each mouse. After 4 days, mice were injected with 100 μg of αCTLA4 (9H10) or 100 μg of αPD-L1 (peritumorally or intraperitoneally). Blood samples were collected in heparinized tubes 5, 7, 9, and 11 days after tumor inoculation. Concentrations of αCTLA4 and αPD-L1 in plasma were measured by ELISA as described above.

Detection of Ab binding to rmFcRn

Ninety-six–well ELISA plates (Greiner Bio-One) were coated with rmFcRn (1 μg/ml; R&D Systems) in PBS at 37°C overnight, followed by blocking with 2% BSA in PBS-T (pH 7.4) for 1 hour at room temperature. Then, wells were washed with PBS-T (pH 7.4) and further incubated with PlGF-$2_{123–144}$–αPD-L1 or unmodified αPD-L1, or human normal IgG (R&D Systems) at increasing concentrations in PBS (pH 6.0 or pH 7.4) for 1 hour at room temperature. After three washes with PBS-T (pH 6.0 or pH 7.4), wells were incubated for 1 hour at room temperature with HRP-conjugated Abs against rat IgG or human IgG in PBS (pH 6.0 or pH 7.4). After three washes with PBS-T (pH 6.0 or pH 7.4), bound Abs were detected with tetramethylbenzidine substrate by measurement of the absorbance at 450 nm and subtracting the absorbance at 570 nm.

Serum cytokine concentration analysis

B16F10 melanoma cells (5×10^5) were injected intradermally on the left side of the back of each 12-week-old C57BL/6 mouse (The Jackson Laboratory). After 4 and 7 days, mice received two doses of 500 μg of αCTLA4 and αPD-L1 peritumorally. On day 9, blood samples were collected in tubes, followed by overnight incubation at 4°C. Cytokine concentrations in serum were measured by Ready-SET-Go! ELISA kits for mouse TNFα and mouse IFN-γ (eBioscience) and mouse IL-2 DuoSet ELISA kit (R&D Systems) according to the manufacturer's protocol.

ALT assays

B16F10 melanoma cells (5×10^5) were injected intradermally on the left side of the back of each 12-week-old C57BL/6 mouse (The Jackson Laboratory). After 4 and 7 days, mice received two doses of 500 μg of αCTLA4 and αPD-L1. On day 9, blood samples were collected in tubes, followed by >4-hour incubation at 4°C. ALT activity in serum was measured by ALT Assay Kit (Sigma-Aldrich) according to the manufacturer's protocol.

Histology

B16F10 melanoma cells (5×10^5) were injected intradermally on the left side of the back of each 12-week-old C57BL/6 mouse (The Jackson Laboratory). After 4 and 7 days, mice were given two doses of 500 μg of αCTLA4 and αPD-L1. Eight and 10 days after tumor inoculation, livers were collected and fixed with 4% PFA. After embedding in paraffin, blocks were cut into 5-μm sections, followed by staining with hematoxylin and eosin. Images were captured with an EVOS FL Auto microscope (Life Technologies). The number of spots of infiltrated lymphocytes was counted by an investigator blinded to the treatment group.

Diabetes monitoring of NOD mice after αPD-L1 treatment

Sixteen-week-old male NOD mice were given 100 μg of αPD-L1 on days 0 and 2. All Ab injections were intradermal in the back skin. Clinical diabetes was defined as a blood glucose concentration of 250 mg/dl for three consecutive days. Blood glucose was measured by AlphaTRAK 2 Glucose Meter (Abbott Animal Health). Blood glucose concentrations were monitored daily from 2 days after initiation of the treatment until 25 days after the initiation of Ab treatment.

B16F10 tumor inoculation and Ab injection

A total of 1×10^6 B16F10-OVA or 5×10^5 B16F10 cells resuspended in 50 μl of PBS were inoculated intradermally on the left side of the back of each C57BL/6 mouse. After 4 (when all tumors were visible and tumor size were around 20 mm^3), 7, or 10 days, mice were injected with 25, 50, 100, or 300 μg of αCTLA4 and/or αPD-L1 intradermally beside the tumor peritumorally or intraperitoneally For distant tumor experiments, 5×10^5 B16F10 cells were injected intradermally on the left side of the back of each mouse on day 0 and on the right side on day 2. On days 4, 7, and 10, mice were injected with 100 μg of αCTLA4 and αPD-L1 (peritumorally or intraperitoneally). Tumors were measured with a digital caliper starting 4 days after the first tumor inoculation, and volumes were calculated as ellipsoids, where $V = 4/3 \times 3.14 \times \text{depth}/2 \times \text{width}/2 \times \text{height}/2$. Mice were sacrificed when either tumor volume had reached over 500 mm^3.

Cell proliferation assay

B16F10 melanoma cells were plated in 24-well plates at a density of 5×10^4 cells per well and incubated overnight at 37°C in Dulbecco's modified Eagle's medium (DMEM) supplemented with 10% fetal bovine serum (FBS). The PlGF-$2_{123–144}$ peptide (1, 10, and 100 μg/ml) was then added. After 3 days of incubation, cell numbers were counted using a hemocytometer.

Tissue and cell preparation and T cell subset analysis

B16F10 melanoma cells (5×10^5) were injected intradermally on the left side of the back of each C57BL/6 mouse. After 4 and 7 days, mice were injected with 100 μg of αCTLA4 and αPD-L1 (peritumorally or intraperitoneally). Mice were sacrificed on day 8. Spleens, LNs, and tumors

were harvested. Tumors were digested in DMEM supplemented with 2% FBS, collagenase D (2 mg/ml), and deoxyribonuclease I (40 μg/ml; Roche) for 30 min at 37°C. Single-cell suspensions were obtained by gently disrupting the organs through a 70-mm cell strainer. Red blood cells were lysed with ACK lysing buffer (Quality Biological). Cells were counted and resuspended in Iscove's modified Dulbecco's medium supplemented with 10% FBS and 1% penicillin/streptomycin (full medium; all from Life Technologies) and used for flow cytometry staining and ex vivo T cell stimulation.

Flow cytometry and Abs

Single-cell suspensions from spleens, LNs, and tumors were prepared as described above. After a washing step, about 2×10^6 cells were used for Ab staining. Abs against the following molecules were used throughout the paper if not otherwise indicated: CD3 (145-2C11, BD Biosciences), CD4 (RM4-5, BD Biosciences), CD8α (53–6.7, BD Biosciences), CD25 (PC61, BD Biosciences), CD45 (30-F11, BD Biosciences), CD44 (IM7, BD Biosciences), CD62L (MEL-14, BD Biosciences), PD-1 (29F.1A12, BioLegend), Foxp3 (MF23, BD Biosciences), IL-2 (JES6-5H4, BD Biosciences), IFN-γ (XMG1.2, BD Biosciences), TNFα (MP6-XT22, eBioscience), and Gzmb (NGZB, eBioscience). Fixable live/dead cell discrimination was performed using Fixable Viability Dye eFluor 455 (eBioscience) according to the manufacturer's instructions. Staining was carried out on ice for 20 min if not indicated otherwise, and intracellular staining was performed using the Foxp3 staining kit according to the manufacturer's instructions (BioLegend). Staining of OVA-specific cells was performed using the SIINFEKL-MHCI pentamer (ProImmune), conjugated with phycoerythrin. For staining, pentamers were diluted 1:10 in PBS containing 2% FBS and incubated for 20 min at room temperature. After a washing step, cells were stained with specific Abs for 20 min on ice before fixation. All flow cytometric analyses were done using a Fortessa flow cytometer (BD Biosciences) and analyzed using FlowJo software (Tree Star).

Ex vivo T cell stimulation

Single-cell suspensions from tumor were prepared as described above. $CD8^+$ T cells were isolated using EasySep kits (STEMCELL Technologies) following the manufacturer's instructions, except that biotinylated αCD105 (12403, BioLegend) was added to the EasySep $CD8^+$ T Cell Isolation Cocktail to remove B16-F10 melanoma cells. Ninety-six–well cell culture plates (BD Falcon) were coated with αCD3 (10 μg/ml; 145-2C11, BioLegend) in PBS overnight at 37°C. Extracted T cells from tumor were plated in 96-well plates and cultured in full medium for 6 hours at 37°C in the presence of αCD28 (2 μg/ml; EL-4, BioLegend) and brefeldin A (5 μg/ml; Sigma-Aldrich). Cells were harvested, stained, and analyzed by flow cytometry as described above.

Tyr:Cre-ER$^+$/LSL-Braf^{V600E}/Pten$^{fl/fl}$ melanoma induction and Ab injection

Eight- to 12-week-old *Tyr:Cre-ER$^+$/LSL-Braf^{V600E}/Pten$^{fl/fl}$* mice were shaved on the back, and 5 μl of 4-OH-tamoxifen (Sigma-Aldrich) at 10 mg/ml was applied topically, as previously described (*24*). Zero, 3, and 6 days after visible tumor development, mice were injected with 100 μg each of αCTLA4 and αPD-L1 peritumorally for a total of three injections. Volume was computed as Volume = Surface × Z, where Surface is computed through ImageJ analysis and Z is the thickness of the tumor, measured with a digital caliper. Mice were sacrificed when tumor volume had reached more than 1000 mm^3.

MMTV-PyMT tumor inoculation and Ab injection

The hair surrounding the mammary glands of FVB mice was shaved. A total of 8×10^5 MMTV-PyMT cells resuspended in 50 μl of PBS were injected subcutaneously into the mammary gland on the right side of each mouse. After 7, 10, or 13 days, mice were injected with 100 μg each of αCTLA4 and αPD-L1 (peritumorally). Tumors were measured with a digital caliper as described above. Mice were sacrificed when tumor volume reached more than 500 mm^3.

Statistical analysis

Statistical significance of differences between experimental groups was calculated with Prism software (version 7, GraphPad). For parametric data, variance between groups was found to be similar by Brown-Forsythe test, and one-way ANOVA followed by Tukey's honestly significant different post hoc test was used for statistical analysis. For nonparametric data, Kruskal-Wallis test followed by Dunn's multiple comparison test was used. For single comparisons, a two-tailed Student's t test was used. Survival curves were analyzed by using the log-rank (Mantel-Cox) test. The n values used to calculate statistics are indicated in figure legends. All experiments were replicated at least twice. The symbols * and ** indicate P values less than 0.05 and 0.01, respectively.

SUPPLEMENTARY MATERIALS

www.sciencetranslationalmedicine.org/cgi/content/full/9/415/eaan0401/DC1

Fig. S1. MALDI-TOF MS analysis revealed that molecular weights are increased by PlGF-$2_{123–144}$ conjugation to αCTLA4 (4F10) and αPD-L1.

Fig. S2. PlGF-$2_{123–144}$ conjugation to αCTLA4 (9H10) and αPD-L1 does not yield aggregates.

Fig. S3. Unmodified αCTLA4 (4F10) and αPD-L1 do not bind to ECM proteins.

Fig. S4. Affinities of PlGF-$2_{123–144}$–αCTLA4 and PlGF-$2_{123–144}$–αPD-L1 for fibronectin and collagen I were measured.

Fig. S5. Affinities of PlGF-$2_{123–144}$–αCTLA4 or unmodified αCTLA4 and αPD-L1 for their antigens were measured.

Fig. S6. Heparin inhibits fibronectin binding of PlGF-$2_{123–144}$–Abs.

Fig. S7. Plasmin cleaves PlGF-$2_{123–144}$.

Fig. S8. PlGF-$2_{123–144}$–Abs are retained in collagen in vitro.

Fig. S9. PlGF-$2_{123–144}$–Abs are retained in the melanoma tissue.

Fig. S10. PlGF-$2_{123–144}$ conjugation does not affect binding of αPD-L1 and FcRn receptor.

Fig. S11. Liver histologies after unmodified and PlGF-$2_{123–144}$–checkpoint blockade Ab treatment are shown.

Fig. S12. PlGF-$2_{123–144}$–Ab treatment extends survival of B16F10 tumor-bearing mice.

Fig. S13. Single-agent treatment with PlGF-$2_{123–144}$–αCTLA4 or PlGF-$2_{123–144}$–αPD-L1 does not affect tumor growth.

Fig. S14. PlGF-$2_{123–144}$ peptide does not affect B16F10 cells' proliferation.

Fig. S15. PlGF-$2_{123–144}$–Ab treatment activates T cells in the spleen.

Fig. S16. PlGF-$2_{123–144}$–Ab treatment activates tumor antigen–specific T cells in tdLN, tested in the B16F10-OVA model.

Fig. S17. Individual tumor growth curves for Fig. 5 are shown.

Table S1. Original data (provided as an Excel file).

REFERENCES AND NOTES

1. P. Sharma, J. P. Allison, The future of immune checkpoint therapy. *Science* **348**, 56–61 (2015).
2. S. L. Topalian, C. G. Drake, D. M. Pardoll, Immune checkpoint blockade: A common denominator approach to cancer therapy. *Cancer Cell* **27**, 450–461 (2015).
3. J. F. Grosso, M. N. Jure-Kunkel, CTLA-4 blockade in tumor models: An overview of preclinical and translational research. *Cancer Immun.* **13**, 5 (2013).
4. M. J. Selby, J. J. Engelhardt, M. Quigley, K. A. Henning, T. Chen, M. Srinivasan, A. J. Korman, Anti–CTLA-4 antibodies of IgG2a isotype enhance antitumor activity through reduction of intratumoral regulatory T cells. *Cancer Immunol. Res.* **1**, 32–42 (2013).
5. T. R. Simpson, F. Li, W. Montalvo-Ortiz, M. A. Sepulveda, K. Bergerhoff, F. Arce, C. Roddie, J. Y. Henry, H. Yagita, J. D. Wolchok, K. S. Peggs, J. V. Ravetch, J. P. Allison, S. A. Quezada, Fc-dependent depletion of tumor-infiltrating regulatory T cells co-defines the efficacy of anti–CTLA-4 therapy against melanoma. *J. Exp. Med.* **210**, 1695–1710 (2013).

6. F. S. Hodi, S. J. O'Day, D. F. McDermott, R. W. Weber, J. A. Sosman, J. B. Haanen, R. Gonzalez, C. Robert, D. Schadendorf, J. C. Hassel, W. Akerley, A. J. M. van den Eertwegh, J. Lutzky, P. Lorigan, J. M. Vaubel, G. P. Linette, D. Hogg, C. H. Ottensmeier, C. Lebbé, C. Peschel, I. Quirt, J. I. Clark, J. D. Wolchok, J. S. Weber, J. Tian, M. J. Yellin, G. M. Nichol, A. Hoos, W. J. Urba, Improved survival with ipilimumab in patients with metastatic melanoma. *N. Engl. J. Med.* **363**, 711–723 (2010).
7. G. J. Freeman, A. J. Long, Y. Iwai, K. Bourque, T. Chernova, H. Nishimura, L. J. Fitz, N. Malenkovich, T. Okazaki, M. C. Byrne, H. F. Horton, L. Fouser, L. Carter, V. Ling, M. R. Bowman, B. M. Carreno, M. Collins, C. R. Wood, T. Honjo, Engagement of the PD-1 immunoinhibitory receptor by a novel B7 family member leads to negative regulation of lymphocyte activation. *J. Exp. Med.* **192**, 1027–1034 (2000).
8. Y. Iwai, M. Ishida, Y. Tanaka, T. Okazaki, T. Honjo, N. Minato, Involvement of PD-L1 on tumor cells in the escape from host immune system and tumor immunotherapy by PD-L1 blockade. *Proc. Natl. Acad. Sci. U.S.A.* **99**, 12293–12297 (2002).
9. C. Blank, T. F. Gajewski, A. Mackensen, Interaction of PD-L1 on tumor cells with PD-1 on tumor-specific T cells as a mechanism of immune evasion: Implications for tumor immunotherapy. *Cancer Immunol. Immunother.* **54**, 307–314 (2005).
10. J. Duraiswamy, K. M. Kaluza, G. J. Freeman, G. Coukos, Dual blockade of PD-1 and CTLA-4 combined with tumor vaccine effectively restores T-cell rejection function in tumors. *Cancer Res.* **73**, 3591–3603 (2013).
11. M. A. Curran, W. Montalvo, H. Yagita, J. P. Allison, PD-1 and CTLA-4 combination blockade expands infiltrating T cells and reduces regulatory T and myeloid cells within B16 melanoma tumors. *Proc. Natl. Acad. Sci. U.S.A.* **107**, 4275–4280 (2010).
12. T. Powles, J. P. Eder, G. D. Fine, F. S. Braiteh, Y. Loriot, C. Cruz, J. Bellmunt, H. A. Burris, D. P. Petrylak, S.-l. Teng, X. Shen, Z. Boyd, P. S. Hegde, D. S. Chen, V. Vogelzang, MPDL3280A (anti–PD-L1) treatment leads to clinical activity in metastatic bladder cancer. *Nature* **515**, 558–562 (2014).
13. S. Spranger, H. K. Koblish, B. Horton, P. A. Scherle, R. Newton, T. F. Gajewski, Mechanism of tumor rejection with doublets of CTLA-4, PD-1/PD-L1, or IDO blockade involves restored IL-2 production and proliferation of $CD8^+$ T cells directly within the tumor microenvironment. *J. Immunother. Cancer* **2**, 3 (2014).
14. J. Larkin, V. Chiarion-Sileni, R. Gonzalez, J. Jacques Grob, C. Lance Cowey, C. D. Lao, D. Schadendorf, R. Dummer, M. Smylie, P. Rutkowski, P. F. Ferrucci, A. Hill, J. Wagstaff, M. S. Carlino, J. B. Haanen, M. Maio, I. Marquez-Rodas, G. A. McArthur, P. A. Ascierto, G. V. Long, M. K. Callahan, M. A. Postow, K. Grossmann, M. Sznol, B. Dreno, L. Bastholt, A. Yang, L. M. Rollin, C. Horak, F. Stephen Hodi, J. D. Wolchok, Combined nivolumab and ipilimumab or monotherapy in untreated melanoma. *N. Engl. J. Med.* **373**, 23–34 (2015).
15. M. M. Martino, P. S. Briquez, A. Ranga, M. P. Lutolf, J. A. Hubbell, Heparin-binding domain of fibrin (ogen) binds growth factors and promotes tissue repair when incorporated within a synthetic matrix. *Proc. Natl. Acad. Sci. U.S.A.* **110**, 4563–4568 (2013).
16. M. M. Martino, F. Tortelli, M. Mochizuki, S. Traub, D. Ben-David, G. A. Kuhn, R. Müller, E. Livne, S. A. Eming, J. A. Hubbell, Engineering the growth factor microenvironment with fibronectin domains to promote wound and bone tissue healing. *Sci. Transl. Med.* **3**, 100ra89 (2011).
17. L. De Laporte, J. J. Rice, F. Tortelli, J. A. Hubbell, Tenascin C promiscuously binds growth factors via its fifth fibronectin type III–like domain. *PLOS ONE* **8**, e62076 (2013).
18. F. Tortelli, M. Pisano, P. S. Briquez, M. M. Martino, J. A. Hubbell, Fibronectin binding modulates CXCL11 activity and facilitates wound healing. *PLOS ONE* **8**, e79610 (2013).
19. L. A. Maile, W. H. Busby, K. Sitko, B. E. Capps, T. Sergent, J. Badley-Clarke, Y. Ling, D. R. Clemmons, The heparin binding domain of vitronectin is the region that is required to enhance insulin-like growth factor-I signaling. *Mol. Endocrinol.* **20**, 881–892 (2006).
20. M. M. Martino, P. S. Briquez, E. Güç, F. Tortelli, W. W. Kilarski, S. Metzger, J. J. Rice, G. A. Kuhn, R. Müller, M. A. Swartz, J. A. Hubbell, Growth factors engineered for super-affinity to the extracellular matrix enhance tissue healing. *Science* **343**, 885–888 (2014).
21. M. J. I. Ansari, A. D. Salama, T. Chitnis, R. N. Smith, H. Yagita, H. Akiba, T. Yamazaki, M. Azuma, H. Iwai, S. J. Khoury, H. Auchincloss Jr., M. H. Sayegh, The programmed death-1 (PD-1) pathway regulates autoimmune diabetes in nonobese diabetic (NOD) mice. *J. Exp. Med.* **198**, 63–69 (2003).
22. Y. Wang, H.-X. Zhang, Y.-P. Sun, Z.-X. Liu, X.-S. Liu, L. Wang, S.-Y. Lu, H. Kong, Q.-L. Liu, X.-H. Li, Z.-Y. Lu, S.-J. Chen, Z. Chen, S.-S. Bao, W. Dai, Z.-G. Wang, Rig-$I^{-/-}$ mice develop colitis associated with downregulation of Gαi2. *Cell Res.* **17**, 858–868 (2007).
23. C. Hörnquist, X. Lu, P. M. Rogers-Fani, U. Rudolph, S. Shappell, L. Birnbaumer, G. R. Harriman, Gαi2-deficient mice with colitis exhibit a local increase in memory $CD4^+$ T cells and proinflammatory Th1-type cytokines. *J. Immunol.* **158**, 1068–1077 (1997).
24. S. Spranger, R. Bao, T. F. Gajewski, Melanoma-intrinsic β-catenin signalling prevents anti-tumour immunity. *Nature* **523**, 231–235 (2015).
25. C. Guy, R. Cardiff, W. Muller, Induction of mammary tumors by expression of polyomavirus middle T oncogene: A transgenic mouse model for metastatic disease. *Mol. Cell. Biol.* **12**, 954–961 (1992).
26. D. M. Lussier, J. L. Johnson, P. Hingorani, J. N. Blattman, Combination immunotherapy with α-CTLA-4 and α-PD-L1 antibody blockade prevents immune escape and leads to complete control of metastatic osteosarcoma. *J. Immunother. Cancer* **3**, 21 (2015).
27. P. A. Ott, F. S. Hodi, C. Robert, CTLA-4 and PD-1/PD-L1 blockade: New immunotherapeutic modalities with durable clinical benefit in melanoma patients. *Clin. Cancer Res.* **19**, 5300–5309 (2013).
28. J. P. Allison, Immune checkpoint blockade in cancer therapy: The 2015 Lasker-DeBakey clinical medical research award. *JAMA* **314**, 1113–1114 (2015).
29. C. Boutros, A. Tarhini, E. Routier, O. Lambotte, F. L. Ladurie, F. Carbonnel, H. Izzeddine, A. Marabelle, S. Champiat, A. Berdelou, E. Lanoy, M. Texier, C. Libenciuc, A. M. M. Eggermont, J.-C. Soria, C. Mateus, C. Robert, Safety profiles of anti–CTLA-4 and anti–PD-1 antibodies alone and in combination. *Nat. Rev. Clin. Oncol.* **13**, 473–486 (2016).
30. The double edge of cancer immunotherapy. *Nat. Med.* **23**, 137 (2017).
31. M. Mellati, K. D. Eaton, B. M. Brooks-Worrell, W. A. Hagopian, R. Martins, J. P. Palmer, I. B. Hirsch, Anti–PD-1 and anti–PDL-1 monoclonal antibodies causing type 1 diabetes. *Diabetes Care* **38**, e137–e138 (2015).
32. M. Okamoto, M. Okamoto, K. Gotoh, T. Masaki, Y. Ozeki, H. Ando, M. Anai, A. Sato, Y. Yoshida, S. Ueda, T. Kakuma, H. Shibata, Fulminant type 1 diabetes mellitus with anti-programmed cell death-1 therapy. *J. Diabetes Investig.* **7**, 915–918 (2016).
33. Y. Miyoshi, O. Ogawa, Y. Oyama, Nivolumab, an anti-programmed cell death-1 antibody, induces fulminant type 1 diabetes. *Tohoku J. Exp. Med.* **239**, 155–158 (2016).
34. M. Fransen, F. Ossendorp, R. Arens, C. J. Melief, Local immunomodulation for cancer therapy: Providing treatment where needed. *Oncoimmunology* **2**, e26493 (2013).
35. M. F. Fransen, M. Sluijter, H. Morreau, R. Arens, C. J. M. Melief, Local activation of CD8 T cells and systemic tumor eradication without toxicity via slow release and local delivery of agonistic CD40 antibody. *Clin. Cancer Res.* **17**, 2270–2280 (2011).
36. M. F. Fransen, T. C. van der Sluis, F. Ossendorp, R. Arens, C. J. M. Melief, Controlled local delivery of CTLA-4 blocking antibody induces $CD8^+$ T-cell–dependent tumor eradication and decreases risk of toxic side effects. *Clin. Cancer Res.* **19**, 5381–5389 (2013).
37. S. Rahimian, M. F. Fransen, J. W. Kleinovink, M. Amidi, F. Ossendorp, W. E. Hennink, Polymeric microparticles for sustained and local delivery of antiCD40 and antiCTLA-4 in immunotherapy of cancer. *Biomaterials* **61**, 33–40 (2015).
38. M. Steiner, D. Neri, Antibody-radionuclide conjugates for cancer therapy: Historical considerations and new trends. *Clin. Cancer Res.* **17**, 6406–6416 (2011).
39. P. Ellmark, S. M. Mangsbo, C. Furebring, P. Norlén, T. H. Tötterman, Tumor-directed immunotherapy can generate tumor-specific T cell responses through localized co-stimulation. *Cancer Immunol. Immunother.* **66**, 1–7 (2017).
40. A. Marabelle, H. Kohrt, C. Caux, R. Levy, Intratumoral immunization: A new paradigm for cancer therapy. *Clin. Cancer Res.* **20**, 1747–1756 (2014).
41. A. Ray, M. A. Williams, S. M. Meek, R. C. Bowen, K. F. Grossmann, R. H. I. Andtbacka, T. L. Bowles, J. R. Hyngstrom, S. A. Leachman, D. Grossman, G. M. Bowen, S. L. Holmen, M. W. VanBrocklin, G. Suneja, H. T. Khong, A phase I study of intratumoral ipilimumab and interleukin-2 in patients with advanced melanoma. *Oncotarget* **7**, 64390–64399 (2016).
42. C. Twyman-Saint Victor, A. J. Rech, A. Maity, R. Rengan, K. E. Pauken, E. Stelekati, J. L. Benci, B. Xu, H. Dada, P. M. Odorizzi, R. S. Herati, K. D. Mansfield, D. Patsch, R. K. Amaravadi, L. M. Schuchter, H. Ishwaran, R. Mick, D. A. Pryma, X. Xu, M. D. Feldman, T. C. Gangadhar, S. M. Hahn, E. J. Wherry, R. H. Vonderheide, A. J. Minn, Radiation and dual checkpoint blockade activate non-redundant immune mechanisms in cancer. *Nature* **520**, 373–377 (2015).
43. K. D. Moynihan, C. F. Opel, G. L. Szeto, A. Tzeng, E. F. Zhu, J. M. Engreitz, R. T. Williams, K. Rakhra, M. H. Zhang, A. M. Rothschilds, S. Kumari, R. L. Kelly, B. H. Kwan, W. Abraham, K. Hu, N. K. Mehta, M. J. Kauke, H. Suh, J. R. Cochran, D. A. Lauffenburger, K. D. Wittrup, D. J. Irvine, Eradication of large established tumors in mice by combination immunotherapy that engages innate and adaptive immune responses. *Nat. Med.* **22**, 1402–1410 (2016).
44. O. A. Ali, S. A. Lewin, G. Dranoff, D. J. Mooney, Vaccines combined with immune checkpoint antibodies promote cytotoxic T-cell activity and tumor eradication. *Cancer Immunol. Res.* **4**, 95–100 (2016).
45. E. F. Zhu, S. A. Gai, C. F. Opel, B. H. Kwan, R. Surana, M. C. Mihm, M. J. Kauke, K. D. Moynihan, A. Angelini, R. T. Williams, M. T. Stephan, J. S. Kim, M. B. Yaffe, D. J. Irvine, L. M. Weiner, G. Dranoff, K. D. Wittrup, Synergistic innate and adaptive immune response to combination immunotherapy with anti-tumor antigen antibodies and extended serum half-life IL-2. *Cancer Cell* **27**, 489–501 (2015).
46. J. A. Joyce, J. W. Pollard, Microenvironmental regulation of metastasis. *Nat. Rev. Cancer* **9**, 239–252 (2009).
47. K. Mimura, K. Sueishi, C. Yasunaga, K. Tanaka, Fibrinolysis activity promotes tumor invasiveness of B16 melanoma cell lines through a reconstituted gel matrix. *Invasion Metastasis* **12**, 24–34 (1991).
48. C. Peters, S. Brown, Antibody-drug conjugates as novel anti-cancer chemotherapeutics. *Biosci. Rep.* **35**, e00225 (2015).

Acknowledgments: We thank T. Gajewski (University of Chicago) for sharing *Tyr:Cre-ER$^+$/LSL-Braf^{V600E}/Pten$^{fl/fl}$* mice and for careful reading of this manuscript, the Human Tissue Resource Center of the University of Chicago for histology analysis, and J. Paz-Montoya and M. Moniatte for MALDI-TOF analysis in the Proteomics Core Facility of EPFL. We also thank X. Quaglia, G. Diaceri, J.-M. Williford, J.-P. Gaudry, P. Briquez, L. Jeanbart, M. Damo, I. van Mier,

S. Gomes, Y. Wang, C. Maulloo, L. Maillat, and M. White for experimental advice and helpful discussions. **Funding:** This work was funded in part by the European Research Commission grant Cytrix. L.P. is funded by the Fonds Pierre-François Vittone. **Author contributions:** J.I. and J.A.H. designed the project. J.I., K.F., and A.I. performed the experiments. J.I., K.F., A.I., M.A.S., and J.A.H. analyzed the data. J.I., K.F., and J.A.H. wrote the paper. H.M.L. contributed to the ECM retention experiments. L.P., P.H., G.G., and M.A.S. assisted with tumor experiments in transgenic mice. **Competing interests:** J.I., K.F., A.I., and J.A.H. are inventors on a U.S. Provisional Patent application no. 62/487,823 that covers the matrix-binding Ab technology presented in this report.

Submitted 5 June 2017
Accepted 27 September 2017
Published 8 November 2017
10.1126/scitranslmed.aan0401

Citation: J. Ishihara, K. Fukunaga, A. Ishihara, H. M. Larsson, L. Potin, P. Hosseinchi, G. Galliverti, M. A. Swartz, J. A. Hubbell, Matrix-binding checkpoint immunotherapies enhance antitumor efficacy and reduce adverse events. *Sci. Transl. Med.* **9**, eaan0401 (2017).

Science Translational Medicine

Matrix-binding checkpoint immunotherapies enhance antitumor efficacy and reduce adverse events

Jun Ishihara, Kazuto Fukunaga, Ako Ishihara, Hans M. Larsson, Lambert Potin, Peyman Hosseinchi, Gabriele Galliverti, Melody A. Swartz and Jeffrey A. Hubbell

Sci Transl Med **9**, eaan0401.
DOI: 10.1126/scitranslmed.aan0401

Keeping immunotherapy closer to home

Immune checkpoint inhibitors are gaining increasing prominence in the field of cancer because of their remarkable success record in many difficult-to-treat tumor types. Unfortunately, activation of the immune system against tumors does not occur in isolation, and these drugs are also associated with a host of immune side effects, which limit their usefulness. To decrease systemic toxicity, Ishihara *et al*. conjugated immune checkpoint antibodies to a matrix-binding peptide and showed that peritumoral injection of these conjugated antibodies results in their retention in tumor tissue, effective antitumor response, and systemic antitumor immunity with fewer adverse effects.

Science Translational Medicine (ISSN 1946-6242) is published by the American Association for the Advancement of Science, 1200 New York Avenue NW, Washington, DC 20005. The title *Science Translational Medicine* is a registered trademark of AAAS.